How Climate Change Affects Extremes in Maize and Wheat Yield in Two Cropping Regions

Caroline C. Ummenhofer,* Hong Xu,[+] Tracy E. Twine,[+] Evan H. Girvetz,[#]
Heather R. McCarthy,[@] Netra Chhetri,[&] and Kimberly A. Nicholas**

* Department of Physical Oceanography, Woods Hole Oceanographic Institution, Woods Hole, Massachusetts
[+] Department of Soil, Water, and Climate, University of Minnesota, St. Paul, Minnesota
[#] International Center for Tropical Agriculture, Nairobi, Kenya, and Nature Conservancy, Seattle, Washington
[@] University of Oklahoma, Norman, Oklahoma
[&] School of Geographical Sciences and Urban Planning, and Consortium for Science, Policy and Outcomes,
Arizona State University, Tempe, Arizona
** Centre for Sustainability Studies, Lund University, Lund, Sweden

ABSTRACT

Downscaled climate model projections from phase 5 of the Coupled Model Intercomparison Project (CMIP5) were used to force a dynamic vegetation agricultural model (Agro-IBIS) and simulate yield responses to historical climate and two future emissions scenarios for maize in the U.S. Midwest and wheat in southeastern Australia. In addition to mean changes in yield, the frequency of high- and low-yield years was related to changing local hydroclimatic conditions. Particular emphasis was on the seasonal cycle of climatic variables during extreme-yield years and links to crop growth.

While historically high (low) yields in Iowa tend to occur during years with anomalous wet (dry) growing season, this is exacerbated in the future. By the end of the twenty-first century, the multimodel mean (MMM) of growing season temperatures in Iowa is projected to increase by more than 5°C, and maize yield is projected to decrease by 18%. For southeastern Australia, the frequency of low-yield years rises dramatically in the twenty-first century because of significant projected drying during the growing season. By the late twenty-first century, MMM growing season precipitation in southeastern Australia is projected to decrease by 15%, temperatures are projected to increase by 2.8°–4.5°C, and wheat yields are projected to decline by 70%. Results highlight the sensitivity of yield projections to the nature of hydroclimatic changes. Where future changes are uncertain, the sign of the yield change simulated by Agro-IBIS is uncertain as well. In contrast, broad agreement in projected drying over southern Australia across models is reflected in consistent yield decreases for the twenty-first century. Climatic changes of the order projected can be expected to pose serious challenges for continued staple grain production in some current centers of production, especially in marginal areas.

1. Introduction

Agroecosystems, which include pasture and cropland, cover nearly 40% of Earth's land surface (Ramankutty and Foley 1999; Asner et al. 2004; Foley et al. 2005) and are increasingly vulnerable to changes in mean climate, its variability and extremes. Modeling these changes accurately at the regional scale is important to prioritize adaptation measures to continue to provide food for a growing global population. Here, we explore how changing climatic conditions in the twentieth and twenty-first centuries affect crop production in two agriculturally important regions: the state of Iowa in the Corn Belt of the Midwest United States, one of the world's most agriculturally dominated and productive regions (Hatfield 2012), as well as a semiarid wheat-growing region in southeastern Australia. Using output from global general circulation models (GCMs) in phase 5 of the Coupled Model Intercomparison Project (CMIP5), we force a dynamic vegetation model to simulate yields for maize in Iowa
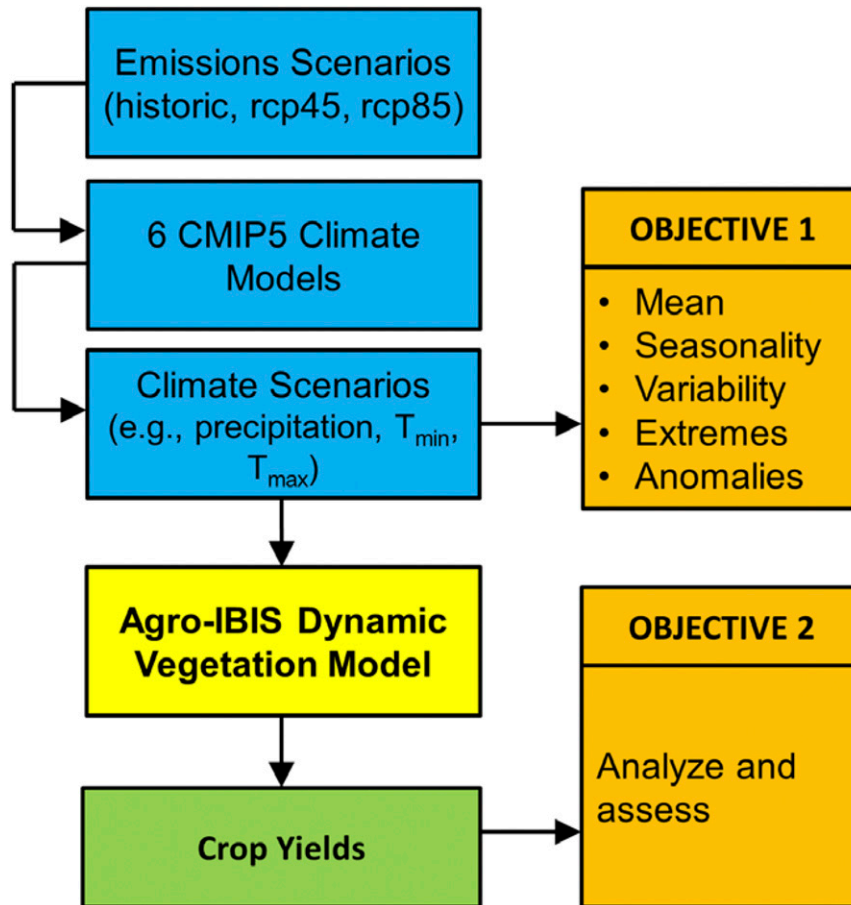
FIG. 1. Flowchart providing a schematic overview of the study's components and the analyses presented.

and wheat in southeastern Australia for historical and projected scenarios. Changes in the mean and variability of hydroclimatic conditions in the two regions are evaluated as to their impact on crop yields. The objectives of this study were to 1) analyze historical and projected means, seasonality, and variability for temperature and precipitation; and 2) analyze how these hydroclimatic variables affect variability in maize and wheat yields in two important cropping regions (Fig. 1).

Previous studies have linked variations in climate to agricultural productivity of cereals around the world on interannual to decadal time scales, such as the El Niño–Southern Oscillation (ENSO) for Australian wheat (Nicholls 1985; Power et al. 1999) and maize in the United States (Malone et al. 2009; Persson et al. 2009) and the North Atlantic Oscillation/Pacific decadal oscillation for maize (Malone et al. 2009) and wheat in the United States (Mehta et al. 2012) and wheat in Europe (Cantelaube et al. 2004; Atkinson et al. 2005).

Crops in the Midwest United States have the benefit of being located in the midlatitudes, a location for which modeling studies predict crop-yield increases, to a point, as mean temperatures rise (Arnell et al. 2002; Southworth et al. 2000, 2002). However, it has been shown that yield increases in response to increasing temperature reach a peak, after which further increases in temperature result in decreases in yield, either directly from plant response to high temperatures or from moisture stress induced by the high temperatures (Cai et al. 2009; Schlenker and Roberts 2009; Lobell et al. 2011a). Recent work on observed climate and crop production trends since the 1980s already found 10% yield declines globally for cereal crops for every 1°C warming, except in high-latitude countries (Lobell et al. 2011b).

Further complicating the interactions of crop production and climate is the potential for increased climate variability in the form of extreme events of flood and drought (e.g., Dai et al. 1998; Dai 2013). The Midwest has sustained the majority of losses because of several of the most costly historic flooding events in the United

States. On the other hand, with most of the region's agriculture being rain fed, the Midwest is highly vulnerable to summer drought, as in 1988 and 2012 (Andresen et al. 2012). Analyzing projections for the Midwest in a range of global and regional climate models, Patricola and Cook (2013) found consistently wetter spring conditions in the twenty-first century, with >66% of the considered models agreeing and a less consistent tendency for drier summers. While climate modeling studies, in addition to mean changes, predict an increase in extreme events in the Midwest United States and other regions in a warming world, less is known about how these events will affect future crop production (Porter and Semenov 2005).

In the context of extremes, "killing degree days" above 29°C for maize are commonly modeled to decrease yields through accelerated growth or direct tissue or enzyme damage (Butler and Huybers 2013). Recent empirical analysis of over 20 000 maize trials in Africa found that each degree day above 30°C reduced the final yield from 1% to 1.7% for optimal rain-fed and drought conditions, respectively (Lobell et al. 2011a). Analysis of U.S. crop data found that increasing temperatures up to 29°C for maize and 30°C for soy increased yields but that temperatures above these thresholds resulted in severe, nonlinear declines in yields: using the Agricultural Production Systems Simulator (APSIM) for maize in the Midwest United States, Lobell et al. (2013) showed a strong negative yield response to temperatures above 30°C and a weak effect of seasonal rainfall, with improved transpiration efficiency at elevated CO_2 levels compensating a small proportion of the negative effects. There is a seasonal dependence, with certain physiological processes more sensitive to temperature, such as the period of sowing to emergence, anthesis, and grain filling, as summarized in a recent review by Sanchez et al. (2014).

Grain-growing regions in southeastern Australia, accounting for 13% of the country's winter crop production (ABARE 2007), are more sensitive to water availability: as Australia's climate is relatively dry and the crop is almost entirely rain fed, water supply is the most critical factor affecting wheat yields overall (French and Schultz 1984). Using APSIM, Wang et al. (2009) found wheat yield across the Murray–Darling basin in Australia's southeast to be closely related to stored soil moisture at the time of sowing and growing season rainfall. The effect of projected climatic conditions on wheat yields across the region in the twenty-first century were assessed by Wang et al. (2011); along a north–south transect, they found warmer sites to be more sensitive to temperature increases, as were drier sites in the west compared to the cooler/wetter east.

While yields in the cooler and wetter sites in the east could benefit from elevated CO_2 levels by 2050, the drier sites in the west were already affected by declining rainfall, which was seen to increasingly affect all but the very wettest sites at higher elevation by 2070 (Wang et al. 2011). Porter and Gawith (1999) review maximum temperature limits for wheat, with certain physiological growth stages exhibiting different temperature sensitivities. Beyond these thresholds, impacts on yield are observed for maximum temperatures above 32°C for sowing to emergence, 31°C for anthesis, and 33°–37°C for grain filling, though, in particular for the latter, temperature sensitivity could differ by up to 35% between cultivars (Porter and Gawith 1999). A recent crop model intercomparison by Asseng et al. (2013) emphasized that crop models need to be improved, in particular their skill to simulate the effects of heat stress on plant growth and wheat yields, with the latter varying more widely in response to temperature variations than to the level of CO_2.

Given the changes in mean climate and its variability, it is important to assess the extremes of the distribution (i.e., years or periods with particularly high or low yields), as they significantly affect the viability of an agricultural enterprise. While recent work has focused on identifying climate extremes and seeking their impact on yields, we define extreme thresholds based on modeled yields directly, allowing the dependent variable to guide further investigation. As such, we propose that this approach is more meaningful for understanding future yield impacts driven by hydroclimatic year-to-year variability, rather than long-term average conditions.

The remainder of the paper is structured as follows: section 2 describes the observational products, climate model output, and the dynamic vegetation agricultural IBIS model (Agro-IBIS). In section 3, cropping and climate characteristics of the two study regions are detailed. The fidelity of historical crop yields simulated in Agro-IBIS is evaluated in section 4. Mean projected changes in yield by the end of the twenty-first century are assessed in section 5, their evolution in section 6. Section 7 details extreme years in crop yield, along with the respective climate anomalies during these years (section 8). Our main findings are summarized in section 9.

2. Datasets and models

a. Observational products

A series of observational and reanalysis products were used, both for the statistical downscaling (cf. section 2b)

TABLE 1. Summary of CMIP5 models used in this study, including the shortened acronym used here, the model's full acronym, and institute.

Shortened acronym	Full model acronym	Institute (country)
CSIRO	CSIRO Mk3.6.0	Commonwealth Scientific and Industrial Research Organization (Australia)
GISS	GISS-E2-R	NASA Goddard Institute of Space Studies (United States)
IPSL	IPSL-CM5A-MR	L'Institute Pierre-Simon Laplace (France)
MIROC	MIROC5	Atmosphere and Ocean Research Institute at the University of Tokyo, National Institute for Environmental Studies, and Japan Agency for Marine-Earth Science and Technology (Japan)
NCAR	CCSM4	National Center for Atmospheric Research (United States)
NOAA	GFDL-ESM2M	NOAA Geophysical Fluid Dynamics Laboratory (United States)

and to assess the representation of the models' climate conditions at the two chosen study locations: Iowa at 42.5°N, 93.75°W and southeastern Australia at 37.5°S, 142.5°E. While each site consists of a single grid point, it is representative of the climatic conditions of the broader region. Observed monthly precipitation data are from the Hulme land precipitation dataset for the period 1900–98 (Hulme 1992, 1994). Minimum and maximum air temperatures (T_{min} and T_{max}) are based on the NOAA–CIRES Twentieth-Century reanalysis, version 2, available for the period 1871–2010 (Compo et al. 2006).

To force Agro-IBIS with observational products, we used weather and climate information derived from a combination of monthly climatic observations and daily, reanalyzed meteorological data on a 0.5° × 0.5° latitude–longitude grid. These driver sets were created by combining 1961–90 climatological mean values and 1901–2005 monthly mean climate data, as given by the University of East Anglia Climate Research Unit datasets (CRU05; New et al. 1999; Mitchell and Jones 2005), with daily anomalies of meteorological data for 1948–2005 from the National Centers for Environmental Prediction–National Center for Atmospheric Research (NCEP–NCAR) reanalysis (Kalnay et al. 1996; Kistler et al. 2001). The monthly average precipitation values of these daily values were mathematically forced to equal the monthly CRU05 values. Using these data, Agro-IBIS calculates hourly values empirically using diurnal relationships of meteorological variables (Campbell and Norman 1998).

b. Climate models

For the two locations, climatic variables used in Agro-IBIS were based on output from six state-of-the-art GCMs generated as part of CMIP5 (Table 1). The representative location of 43.25°N, 93.25°W was chosen for Iowa and, for southeastern Australia, 36.75°S, 142.25°E (as the closest grid point location to the observed; for further details, see section 3). Monthly bias-corrected

CMIP5 output was analyzed for the following three scenarios: historical, RCP4.5, and RCP8.5. RCP4.5 and RCP8.5 refer to the representative concentration pathways (Moss et al. 2010; Riahi et al. 2011), where the radiative forcing in 2100 will be approximately 4.5 W m^{-2} and 8.5 W m^{-2} higher, respectively, than in the preindustrial period. RCP4.5 is a stabilization scenario, where radiative forcing peaks by 2100, while RCP8.5 is a scenario of very high greenhouse gas emissions, where radiative forcing does not peak by 2100 (IPCC 2013). For consistency, an equal number of years was analyzed for each scenario: that is, 1910–2005 for the historical and 2006–2100 for the future projections (RCP4.5 and RCP4.5). Only one ensemble member (r1i1p1) was used for each model.

DOWNSCALING

The climate model data for all locations were bias corrected (downscaled) using quantile mapping to historical climate data at a 0.5° grid cell resolution (cf. section 2a). The bias correction was conducted using the R statistical program contributed package qmap, which performs a quantile mapping using robust empirical quantiles (Gudmundsson et al. 2012). Interpolation beyond the range of the historical distribution was conducted using a linear interpolation suggested by Boé et al. (2007). All results shown and discussed for the GCMs in this study are after bias correction and downscaling.

c. Agro-IBIS model simulations

Agro-IBIS is a dynamic global vegetation model adapted from the Integrated Biosphere Simulator (Foley et al. 1996; Kucharik et al. 2000) to simulate the growth and management of food (Kucharik and Brye 2003) and bioenergy crops (VanLoocke et al. 2010, 2012), as well as the growth of natural vegetation. The model's hierarchical structure simulates fast-response processes that vary hourly, such as energy, water,

carbon, and momentum balance of the vegetation canopy and soil; processes that vary daily such as leaf growth; and slow-response processes like soil carbon storage and turnover. Agro-IBIS was developed to capture key differences in C3 and C4 crop physiology, phenology, and carbon allocation. Net primary productivity is simulated at each model step by scaling the net effects of photosynthesis and autotrophic respiration to the canopy. For C3 species, the model uses a widely tested semimechanistic model for photosynthesis (Farquhar et al. 1980) and an empirical model for stomatal conductance (Ball et al. 1987). For C4 species, Agro-IBIS uses a coupled model of photosynthesis and stomatal conductance (Collatz et al. 1992; Farquhar and Sharkey 1982). Agro-IBIS simulates the growth stages of crops, including planting, emergence, grain or pod fill, senescence, and harvest, according to accumulated growing degree-days (GDD). When accumulated GDD thresholds are reached, the crop transitions from one growth stage to the next, and with this come shifts in carbon allocation to leaves, stems, roots, and reproductive systems. The fraction of carbon allocated to leaves, stems, and roots decreases after peak leaf area index is reached and eventually reaches zero, while allocation to reproductive systems increases to 1. Through its physiological and phenological algorithms, crops in Agro-IBIS will respond to changes in temperature by changing carbon assimilation rates either directly because of changes in temperature, or indirectly because of induced moisture stress, and by changing simulated planting dates and transitioning to growth stages at different times as GDD are accumulated more or less rapidly. Changes in all of these processes contribute to changes in crop yield by either changing the magnitude of carbon assimilation or changing crop duration. For more information on Agro-IBIS processes and parameters, please see Kucharik and Brye (2003), Kucharik (2003), and Twine et al. (2013). The model is responsive to management options (e.g., irrigation, fertilizer application, and planting date) and environmental stresses (e.g., temperature, moisture, radiation, and humidity). Input requirements include soil texture class at each of 11 soil layers with variable depths, solar radiation or cloud cover, air temperature, precipitation, humidity, and wind speed.

Agro-IBIS has been successfully evaluated for its simulation of crop yields (Kucharik 2003), leaf area index, gross primary productivity (Twine and Kucharik 2008; Schaefer et al. 2012), and surface energy balance (Kucharik and Twine 2007; Webler et al. 2012). The model has also been used to evaluate impacts of nitrogen leaching on nitrate export in the Mississippi River basin (Donner et al. 2002; Donner and Kucharik 2008), trends in productivity in the twentieth century (Twine and Kucharik 2009), climate-regulation services of natural and agricultural ecoregions throughout the Western Hemisphere (Anderson-Teixeira et al. 2012), and effects of trends in planting date and cultivar on yields and surface energy balance (Sacks and Kucharik 2011).

SIMULATIONS WITH OBSERVATIONS AND CLIMATE MODEL OUTPUT

To evaluate the ability of the model to capture historic crop yields, we first ran Agro-IBIS with observation-based climate datasets at each of our sites. At the U.S. site, the nitrogen fertilizer application rates were input at historic rates that increased nearly linearly from $3.5 \, kg \, ha^{-1}$ in 1950 to $135 \, kg \, ha^{-1}$ in 1985, then continuing at $135 \, kg \, ha^{-1}$ until 2005. As historic nitrogen fertilizer application rates were unavailable at the southeast Australian site, we used fixed $43 \, kg \, ha^{-1}$ (FAO 2012). Historic simulated maize yield for 1951–2005 at the U.S. site was evaluated against reported yields based on crop-yield surveys for the counties contained within the model grid cell (USDA-NASS 2009); the simulated wheat yield for 1982–2000 at the southeast Australian site was evaluated against a gridded global yield dataset derived by combining yield survey and remotely sensed net primary production (NPP; Iizumi et al. 2014). Yield data from the grid cell that is closest to our site were used in the comparison.

We then drove Agro-IBIS with bias-corrected GCM output for the twenty-first century. Unlike in the runs to validate Agro-IBIS, nitrogen fertilizer application rates were held constant for the entire run with GCM output at a present-day value of $135 \, kg \, ha^{-1}$ at the U.S. site (USDA 2013) and $43 \, kg \, ha^{-1}$ at the southeast Australian site (FAO 2012) in order to assess the response of yield to changes in climate only. The maize cultivar was fixed at requiring 1700 GDD (base temperature $= 10°C$) to maturity, and winter wheat was fixed at requiring 2200 GDD (base temperature $= 0°C$) to maturity. In addition, we used prognostic planting dates. For maize, the planting date was determined as the date when 10-day average temperature was higher than 10°C and the 10-day average T_{min} was higher than 6°C. For winter wheat, the planting date was determined as the date when 5-day average T_{min} dropped below 5°C.

In all model runs, Agro-IBIS was forced with information on soil texture class that varies by depth from the surface to 2.5 m. For the U.S. site, soil texture for 11 soil layers was input from the conterminous United

States multilayer soil characteristics database (CONUS-SOIL; Miller and White 1998), which is based on the State Soil Geographic Database (STATSGO) soil survey. For the Australian site, soil texture was determined from the International Geosphere–Biosphere Program (IGBP 2000) global soil dataset. Although Agro-IBIS simulates the response of C3 and C4 crops to increasing CO_2 concentrations (Twine et al. 2013), in this study we held CO_2 constant at mid-twentieth century levels in all runs to isolate the indirect effects of climate change on crop yield.

3. Cropping/climate characteristics of study regions

a. Site selection and description

Two different locations were selected for this study, representative of the larger regions, both in regard to climate and cropping characteristics. The first location is in central Iowa at 43°N, 93°W, where maize cropping is prevalent. For the second location, a dominant wheat-cropping region in southeastern Australia was chosen: 37°S, 142°E in the Wimmera in western Victoria northwest of Melbourne. Throughout the remainder of the study, the seasons we refer to are specific to the respective hemisphere, without the addition of ''boreal'' and ''austral'' in each instance. The term ''growing season'' refers to the period May–September and June–October in Iowa and southeastern Australia, respectively.

Located in the U.S. Midwest Corn Belt, Iowa is dominated by its continental location: summers are influenced by the incursion of warm, humid tropical airmasses, while the position and configuration of the polar jet stream exerts the dominant climatic influence throughout the remainder of the year (Andresen et al. 2012). Iowa is ranked first in the nation for acres of maize for grain (USDA-NASS 2009) and showed the highest yield per harvested acre in 2011. Maize is grown as a summer crop, with the most active planting occurring between 25 April and 18 May. Harvest usually occurs between 5 October and 9 November. While precipitation during the growing season (May–September) plays a major role in influencing year-to-year variability in maize yield, studies have shown that over longer time scales, maize yields are negatively correlated with temperature (Lobell and Asner 2003; Lobell and Field 2007; Twine and Kucharik 2009). Therefore, increasing average temperatures have likely already limited maize yield in Iowa and will likely continue to contribute to reductions in potential maize yield.

The Wimmera region in southeastern Australia is an important grain-growing region, which lies in the Australian premium white wheat area. Together with the Mallee region to the north, it accounts for 75% of Victoria's wheat production (DEPI 2012), with the latter providing 11% of the total Australian wheat production (2008–13 average; ABARE 2013). The climate of the broader Wimmera region is characterized by hot summers and mild winters. Wheat is grown as a winter crop, with sowing mostly in May and June, but ranging from as early as April under ideal conditions to as late as August in extreme dry conditions (Stephens and Lyons 1998). The arrival of the autumn break, the first good rainfall of the autumn season, is thus keenly anticipated to allow for sowing, and its delay or failure can severely impact crop yields (Pook et al. 2009). As in maize, increasing daily maximum temperatures have been associated with decreases in wheat yield (Porter and Gawith 1999), though rising minimum temperatures and reduced frosts have been linked to increased wheat yields in Australia (Nicholls 1997).

b. Historical and projected climate in Iowa

The observed seasonal cycle in precipitation in Iowa is characterized by a minimum during winter (30 mm month^{-1}) and increased precipitation during May through September (60–160 mm month^{-1}; Fig. 2). After downscaling, all six models in the historical scenario have a realistic representation of the observed seasonal cycle in precipitation and lie within ±1 standard deviation of the mean observed seasonal cycle (gray shading in Fig. 2), with the exception of underestimating rainfall during the wintertime minimum (November–February). Changes in precipitation projected for the future scenarios are generally small, with little difference between the RCP4.5 and RCP8.5 scenarios. There is, however, a tendency across models toward increased spring rainfall in future, and possibly a slight reduction during summer in some models (Figs. 2g,j), consistent with previous findings (e.g., Patricola and Cook 2013).

Mean observed T_{min} in Iowa centers on −11°C in January and +18°C in July, with little interannual variability (Fig. 2). In the historical scenario, all models lie within this variability for T_{min}. Mean Iowa T_{min} is projected to rise by 2°–3°C in the future, with slightly higher values in RCP8.5 than for RCP4.5 (e.g., Fig. 2b). The projected increases seem to be largest during winter and summer and smaller during spring and autumn.

The mean observed T_{max} lies around −4°C in January and +28°C in August, both well captured within the interannual observed variability in the historical simulation by the models (Fig. 2). Projected increases in
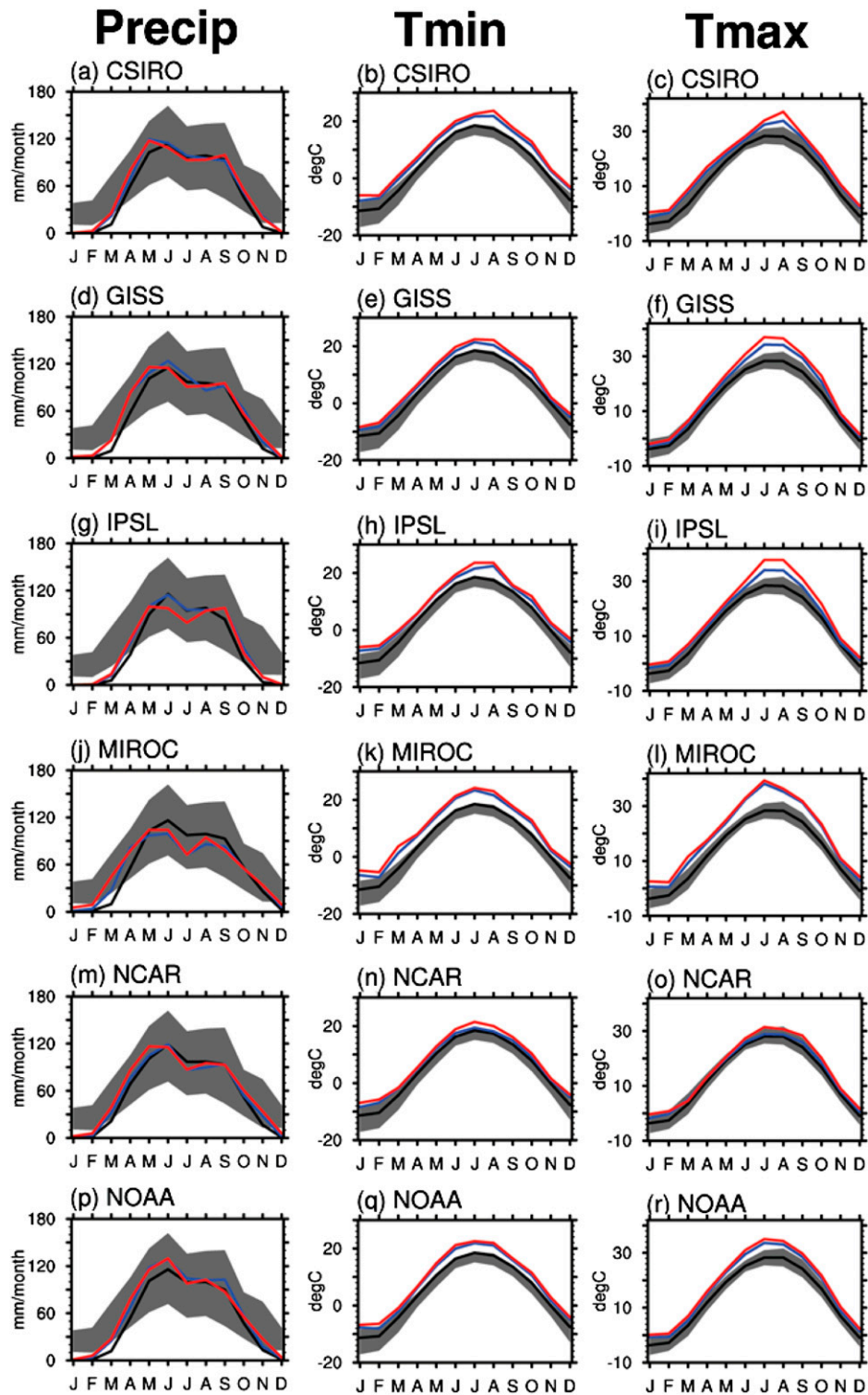
FIG. 2. Seasonal cycle of (left) precipitation (mm month^{-1}), (middle) T_{min} (°C), and (right) T_{max} (°C) in Iowa in models for different scenarios: historical (black), RCP4.5 (blue), and RCP8.5 (red). The gray shading represents the ±1 std dev around the observed mean seasonal cycle for the respective variable.
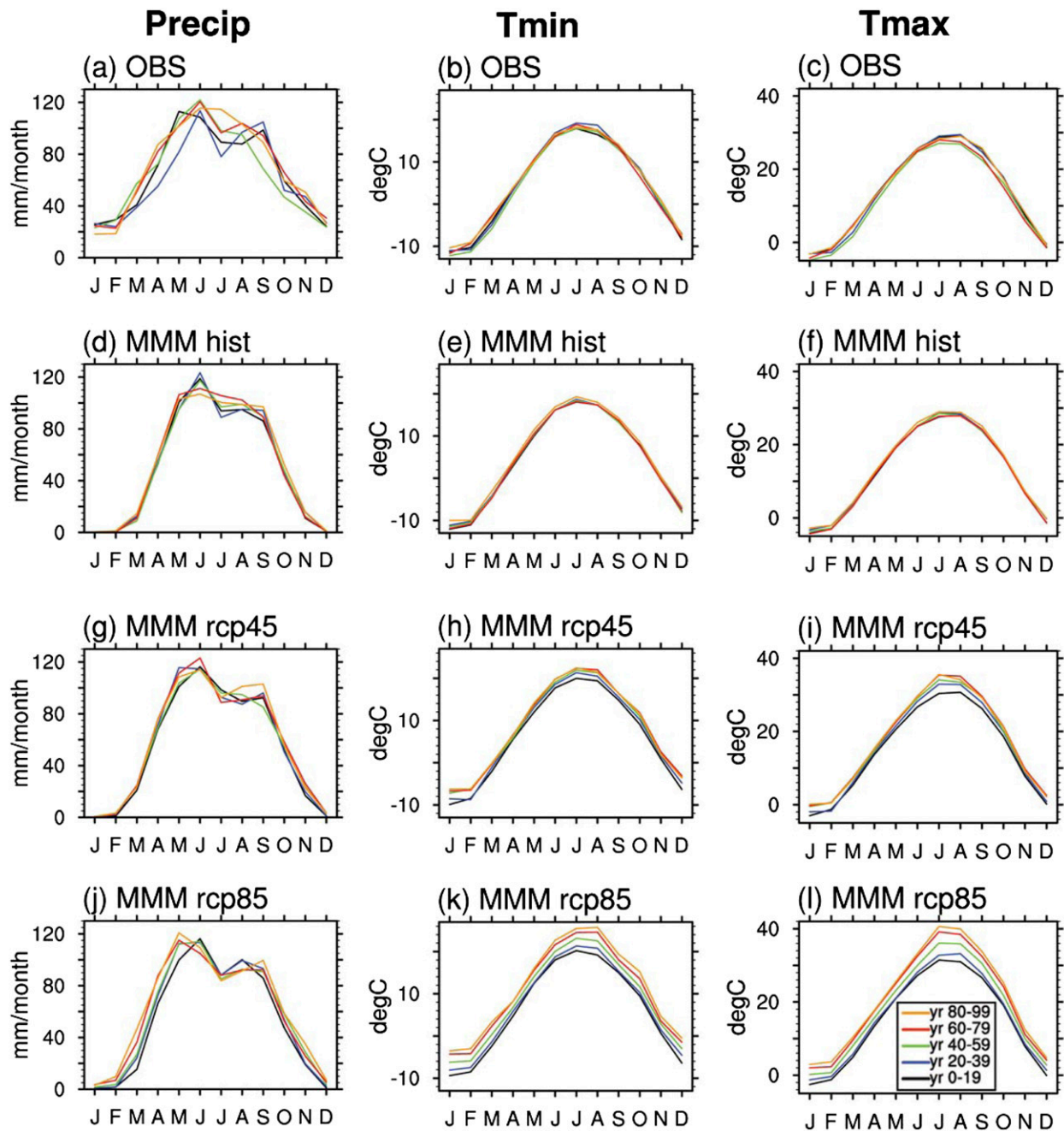
FIG. 3. Seasonal cycle of observed and multimodel mean of (left) precipitation (mm month^{-1}), (middle) T_{min} (°C), and (right) T_{max} (°C) for Iowa, shown for the observations compared with the three scenarios (historical, RCP4.5, and RCP8.5) for different 20-yr periods indicated in color [see key in (l)].

mean T_{max} range between 2°–5°C for different models and seasons. Increases during summertime are particularly pronounced for July and August in the GISS, IPSL, and MIROC models (Figs. 2f,i,l). Several models project a considerable difference in the T_{max} rise between the RCP4.5 and RCP8.5 scenarios (e.g., CSIRO and IPSL; Figs. 2c,i).

It is of interest to explore changes in the observed and simulated seasonal cycle of precipitation and temperatures in Iowa over time. Figure 3 shows the seasonal cycle for different 20-yr periods for the twentieth century for observations, and the multimodel mean (MMM) in the three different scenarios (historical, RCP4.5, and RCP8.5). The observed seasonal cycle in

precipitation is characterized by considerable decadal variability, but there is an indication of slight increases in precipitation during spring and summer in the latter half of the twentieth century, compared to earlier 20-yr periods (Fig. 3a). The seasonal cycle of precipitation in the MMM historical scenario broadly agrees with the observed seasonal distribution and magnitudes (Fig. 3d), but the simulated seasonal cycle is slightly amplified and more narrowly confined to the April–October months and exhibits less decadal variability. Furthermore, winter precipitation (November–February) is underestimated in the MMM compared to the observed (Figs. 3a,d). Projected changes in precipitation for Iowa by the end of the twenty-first century are small in the RCP4.5 scenario (Fig. 3g). In contrast, for the RCP8.5 scenario, increased precipitation is projected for the March–May (MAM) months, with lower rainfall later in the season in August–September by the end of the twenty-first century (Fig. 3j), consistent with Patricola and Cook (2013).

For T_{min}, the seasonal cycle for the observed and MMM are in close agreement, varying between $-10°C$ in winter and $+15°C$ in summer, with little decadal variability (Figs. 3b,e). For the twenty-first century, projections of T_{min} show increasingly higher temperatures toward the end of the century in the RCP4.5 and RCP8.5 scenarios (Figs. 3h,k), with higher increases in RCP8.5: T_{min} values at the end of the twenty-first century in RCP8.5 are up to 6°C higher during winter and summer, and slightly less during spring and autumn, compared to the start of the century (Fig. 3k). Even greater changes are seen for T_{max}, with the MMM seasonal cycle at the end of the twenty-first century approaching 40°C in the RCP8.5 scenario for Iowa (Fig. 3l).

c. Historical and projected climate in southeastern Australia

Precipitation in southeastern Australia at 37°S, 142°E is characterized by enhanced cool-season rainfall, predominantly during May–September. Observed winter [June–August (JJA)] precipitation has a mean of ~70 mm month^{-1}, while mean summer [December–February (DJF)] precipitation is ~35 mm month^{-1} (Fig. 4a). After downscaling, the models largely capture the observed seasonal cycle in precipitation (Fig. 4). One exception is the IPSL model, which has a tendency for overly uniform rainfall throughout the year and thus has a dry bias during JJA (Fig. 4g). Projections for the twenty-first century across models indicate a decrease in precipitation, especially pronounced in spring (e.g., Fig. 4p). There is also a hint of reduced precipitation in late autumn in several models in the twenty-first century (e.g., Figs. 4g,p), with autumn being the season with the

largest observed rainfall decline in recent decades (Timbal and Drosdowsky 2013, and references therein). The recent (and projected) precipitation decline in autumn has large implications for the region's agricultural productivity, given the importance of the autumn break for sowing of winter wheat (Pook et al. 2009).

The seasonal cycle in observed T_{min} varies between 16°C in DJF and 6°C in JJA (Fig. 4b). All models in the historical scenario capture the observed seasonal cycle in T_{min} well. Mean projected increases in T_{min} in the twenty-first century are on the order of 2°–3°C across the models. There is some seasonality to the projected T_{min} increase, with larger values seen in winter and summer, but there is some inconsistency amongst models. The mean observed T_{max} lies between 27°C in summertime and lows of 12°C during winter (Fig. 4c). The observed T_{max} seasonal cycle is well represented in the models' historical scenario. Projected increases in T_{max} are comparable in size and seasonality to the projections of T_{min}. Consistent increases in projected T_{max} outside the observed variability are seen across the models, especially in JJA (Fig. 4).

The development of the seasonal cycle in precipitation and temperatures is further assessed in Fig. 5 in the MMM for southeastern Australia. Given the range in the observed seasonal cycles in precipitation for the different 20-yr periods, it is clear that the region experiences substantial decadal variability in rainfall (Fig. 5a; Pook et al. 2009). There is an indication of reduced rainfall in recent decades in late autumn, consistent with earlier work (e.g., Cai and Cowan 2008, 2013; Timbal and Drosdowsky 2013) and associated with tropical sea surface temperatures and associated wave train response, a poleward shift of maximum baroclinicity, and changes in the subtropical ridge, respectively. While the historical and RCP4.5 scenarios in the MMM do not clearly reflect this decline in autumn precipitation (Figs. 5d,g), it is apparent in RCP8.5 (Fig. 5j). The MMM seasonal cycle in RCP8.5 overall projects drier conditions toward the end of the twenty-first century in southeastern Australia, particularly during autumn and spring, in line with earlier findings for phase 3 of the Coupled Model Intercomparison Project (CMIP3) models (e.g., Pitman and Perkins 2008).

The seasonal cycle in T_{min} indicates a rise in recent decades in the observed, compared to the start of the twentieth century, predominantly during austral summer and the second half of the year (Fig. 5b). This is not well reproduced in the historical scenario (Fig. 5e). Projections of T_{min} by the end of the twenty-first century show a substantial rise in temperature of 1°–2°C throughout the year for RCP4.5 and in excess of 3°C for RCP8.5 (Figs. 5h,k). The development of T_{max} mirrors that for T_{min}, in that the 1°–2°C summertime rise in
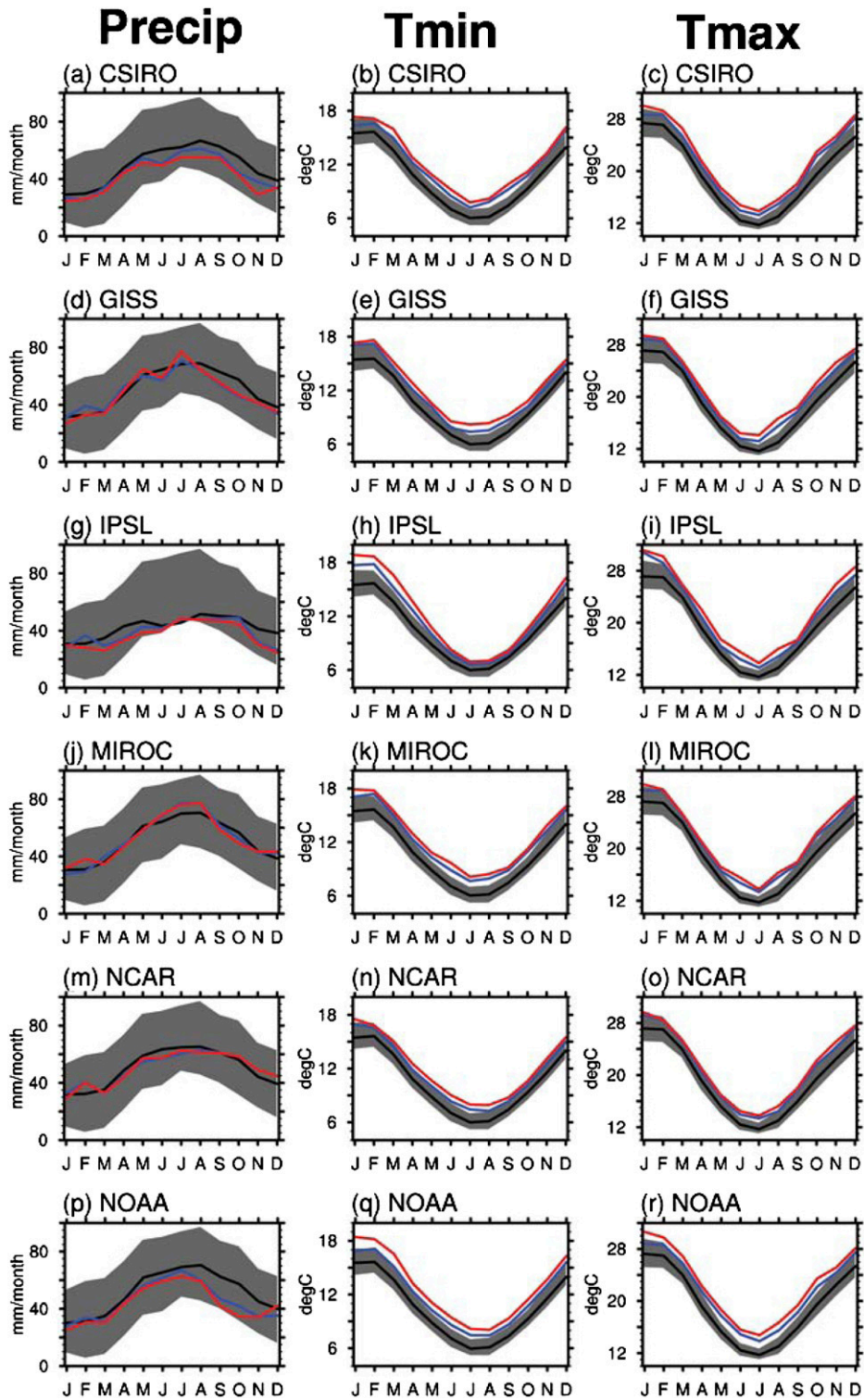
FIG. 4. Seasonal cycle of (left) precipitation (mm month^{-1}), (middle) T_{min} (°C), and (right) T_{max} (°C) in southeastern Australia in models for different scenarios: historical (black), RCP4.5 (blue), and RCP8.5 (red). The gray shading represents the ±1 std dev around the observed mean seasonal cycle for the respective variable.
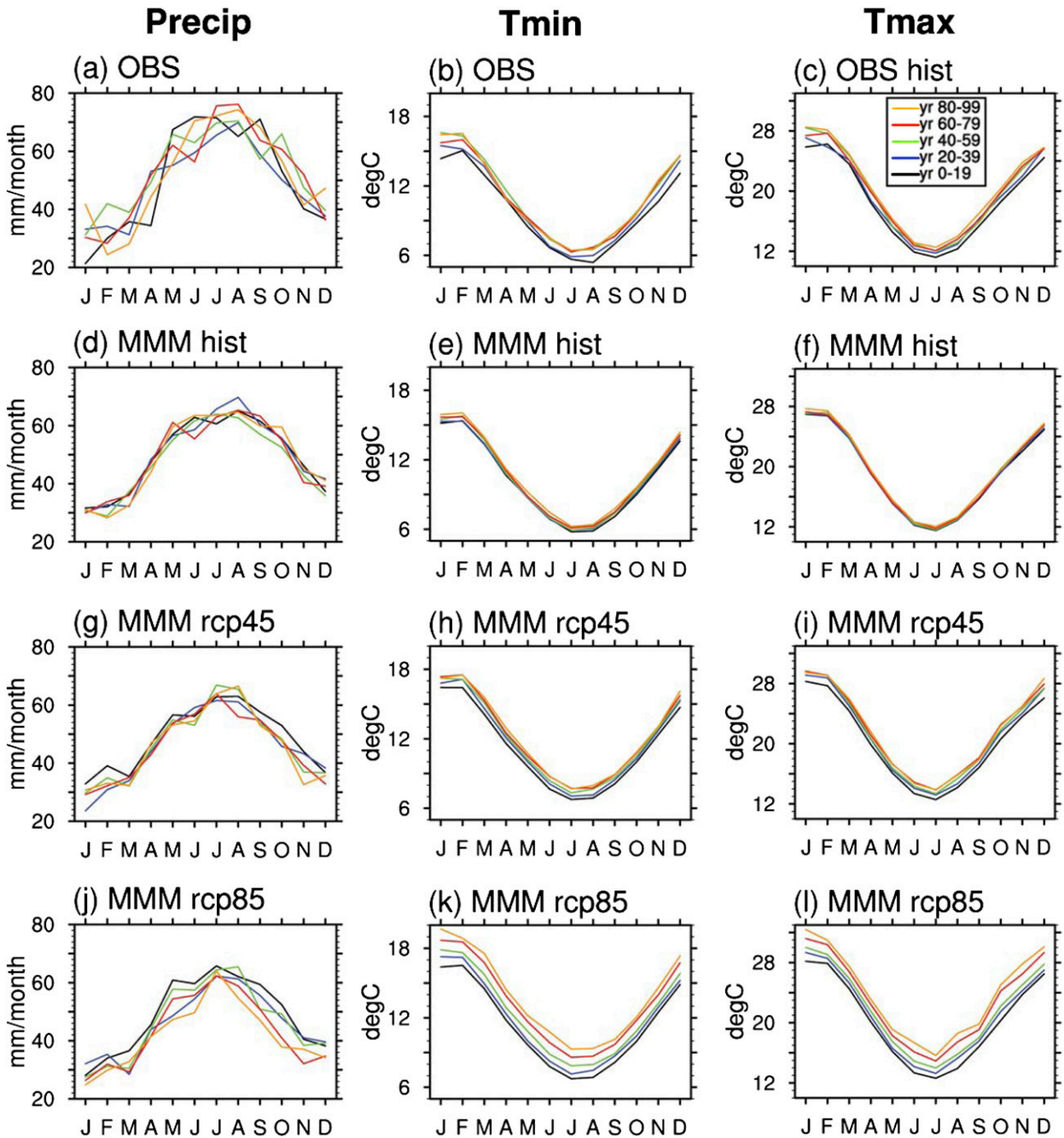
Precip   Tmin   Tmax

FIG. 5. Seasonal cycle of observed and multimodel mean of (left) precipitation (mm month^{-1}), (middle) T_{min} (°C), and (right) T_{max} (°C) for southeastern Australia, shown for the three scenarios (historical, RCP4.5, and RCP8.5) for different 20-yr periods indicated in color [see key in (c)].

observed recent decades is not reflected in the historical MMM (Figs. 5c,f). Using a range of CMIP3 models to assess T_{max} and T_{min} over Australia, Perkins et al. (2009) found that less skillful models (i.e., those that showed less skill in representing twentieth century conditions) overall simulated enhanced warming for the twenty-first

century compared to those that were more skillful, which showed more moderate warming. This needs to be kept in mind for interpreting the T_{max} increase of 1°–2°C by the end of the twenty-first century in RCP4.5 and in excess of 3°C warming projected in RCP8.5 (Figs. 5i,l) and their potential impacts on yield.
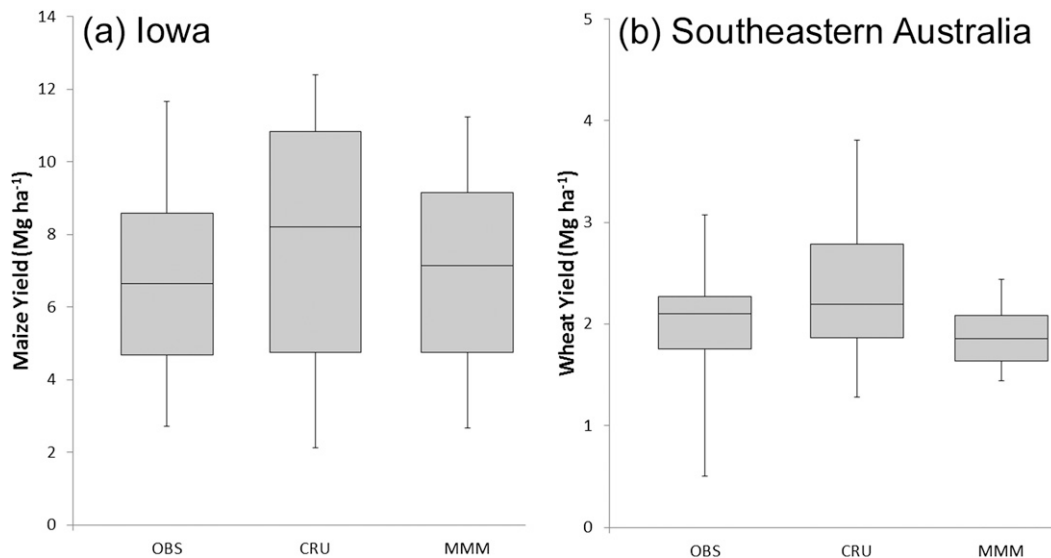
FIG. 6. Box-and-whisker plot of observed and simulated yield (Mg ha^{-1}) for (a) maize in Iowa and (b) wheat in southeastern Australia. Shown are the observations (OBS) from USDA-NASS (2009) for Iowa and Iizumi et al. (2014) for southeastern Australia, the Agro-IBIS run with observed climate variables from the CRU dataset (CRU), and the Agro-IBIS run with multimodel mean (historical scenario) from six downscaled GCMs. The box is delimited by the 25th and 75th percentile, with the median indicated as the line in between; the whiskers correspond to minimum and maximum values.

4. Agro-IBIS evaluation

The dynamic vegetation model Agro-IBIS was evaluated to ensure its suitability for the present study. At the U.S. site, Agro-IBIS driven with observation-based climate data (CRU) simulated a median maize yield of 8.2 Mg ha^{-1} over the past 50 years, slightly higher than the 6.7 Mg ha^{-1} observed (Fig. 6a). We expect observed historic yield to be somewhat overestimated in the model because of the relatively high GDD requirement for maturity in the model and the lack of representation of real-world stresses (e.g., weeds, pests, and differences in farmer management). We chose a GDD requirement in the upper range of cultivars reported for this region (Neild and Newman 1987), because currently this should simulate greater yield than a lower GDD requirement. In the future, more rapid GDD accumulation with increases in temperature could lead to shorter crop duration and limit yields, and we want to quantify this predicted effect. The Pearson correlation coefficient between observed yield and that simulated with the observation-based climate data is 0.83 (p < 0.001; not shown), suggesting that the model captures year-to-year variability in yield well. This is also borne out by the comparable minimum and maximum yield values, as well as the interquartile range in Fig. 6a. When the model was driven with downscaled GCM output for the historic scenario, the simulated yield was close to observed yields with

a median yield of 7.1 Mg ha^{-1} for the MMM, compared with the observed 6.7 Mg ha^{-1} (Fig. 6a).

At the southeast Australian site, Agro-IBIS captured the overall magnitude of the wheat yield. The 19-yr median yields simulated with CRU data and GCM output were 2.2 Mg ha^{-1} and 1.9 Mg ha^{-1} in the MMM, respectively, compared with the reported 2.1 Mg ha^{-1} (Fig. 6b). This also seems to be consistent with the average 2.3 Mg ha^{-1} in 2011 reported by the Department of Environment and Primary Industries (DEPI 2012) for the Wimmera region and falls within the range of yields presented by Asseng et al. (2013) for Australia. While the interquartile range of simulated wheat yield for the MMM is in agreement with observations, it is larger and skewed toward higher yield values when forcing Agro-IBIS with CRU data. This can be explained by several reasons: First, the grid cell of the historic yield dataset used in the comparison does not completely overlap with our grid cell as a result of its different spatial resolution; given the meridional gradient in precipitation in this region, this can affect yields obtained. Second, the yield dataset was derived based on yield statistics and satellite-derived NPP. As such, the evaluation yield dataset for the southeastern Australian site has greater uncertainty than the one at the U.S. site, which was based on crop-yield surveys for the counties in the model grid cell (USDA-NASS 2009). Third, as in the maize simulation, Agro-IBIS is not able to capture all

the real-world stresses that might have an impact on the actual yield. Notwithstanding these caveats, our evaluation suggests that Agro-IBIS is sensitive to climatic variations, adequately represents observed yield statistics at our two sites, and is an effective tool to assess the impact of a changing climate on crop yield.

5. Changes in mean climate and crop yield

Having evaluated the climate and crop model to our satisfaction, for the remainder of the study, we assessed output from the Agro-IBIS simulations forced with downscaled GCM output for the historical, RCP4.5, and RCP8.5 emissions scenarios, as described in section 2c. It is of interest to assess the effect on year-to-year crop-yield anomaly that projected growing season changes in precipitation and temperature will have in the twenty-first century, relative to a historical baseline. In Fig. 7, year-to-year percent anomaly in crop yield is shown in relation to temperature and precipitation changes individually, as well as in combination, for individual years in the period 2071–2100, compared to a historical baseline average of 1951–80 (for all GCMs and emission scenarios). For both Iowa and southeastern Australia, we found that increases in temperature negatively affected yields (Figs. 7a,b), while increases in precipitation positively affected yields (Figs. 7c,d). Generally speaking, based on the slope of the lines in Fig. 7 (all highly statistically significant at $p < 0.01$), a temperature increase of 1°C resulted in a yield decrease of 10% in Iowa and 15% in southeastern Australia (Figs. 7a,b). In contrast, a precipitation increase of 10 mm month^{-1} resulted in a 12% rise in yield in Iowa and a 9% rise in Australia (Figs. 7c, d). With this said, the specific change in yield will depend on the interaction of both temperature and precipitation and their timing, which we will further assess in the following sections.

It is also apparent from Fig. 7 that changes in temperature and precipitation during the growing season work together to impact crop yields; however, their effects are not additive. Their combined effects on crop yield are shown in Figs. 7e,f as a percentage change in the yield achieved in individual years during the period 2071–2100 in the RCP4.5 and RCP8.5 scenarios, relative to the 1951–80 baseline in the historical run.

Overall changes in crop yield by the end of the twenty-first century (2071–2100) compared to a baseline for the 1951–80 period in the historical run are shown in Fig. 8. For Iowa, the median increase in crop yield in the RCP4.5 scenario is 6% across the six GCMs, while a median yield decrease of −21% is recorded for RCP8.5

(Fig. 8a). In contrast, for southeastern Australia, median yield decreases by close to −50% and −75% for RCP4.5 and RCP8.5, respectively (Fig. 8b). The projected wheat yield decreases in southeastern Australia here are larger than the changes found by Potgieter et al. (2013), who reported decreases of −5% to −30% for inland Victoria. However, their analysis period of 2020–50, compared to the period 2071–2100 used here, likely accounts for some of the differences in projected yield change.

6. Evolution of crop-yield distribution

a. Iowa

Because yield is a function of carbon accumulation in the crop throughout its growth, we analyzed monthly NPP in order to understand how the crop responds to changes in climate at various stages of its growth and to evaluate how the timing of extremes in climate can affect yield. Figure 9 shows the evolution of the seasonal cycle in NPP in Iowa for maize for 20-yr periods in the MMM and for individual models for the historical, RCP4.5, and RCP8.5 scenarios. The MMM of NPP in the historical scenario is 0 during the winter months, starts increasing in May with the start of the growing season, reaching 0.4 kg m^{-2} in July, and decreasing sharply thereafter (Fig. 9a). There is good agreement in overall shape amongst models. However, slightly higher peak NPP rates during JJA are seen with GISS and NOAA (Figs. 9g,s), with lower values in IPSL (Fig. 9j), and an (earlier) shift by 1–2 months in the NCAR model (Fig. 9p). The MMM seasonal cycle of NPP does not differ much from one 20-yr period to another for the historical scenario (Fig. 9a). In contrast, there is some decadal variability in NPP apparent in individual models, in particular for CSIRO, IPSL, and MIROC (Figs. 9d,j,m). The NOAA model hints at small increases in NPP during autumn (August–October) toward the end of the historical run, compared to earlier 20-yr periods (Fig. 9s), potentially related to coincident late-summer increases in Iowa precipitation in that model (figure not shown).

The projected NPP in Iowa in July in the MMM for the RCP4.5 scenario is lower at the end of the twenty-first century, compared to earlier 20-yr periods, and NPP remains reduced for the August–October period (Fig. 9b). For the RCP4.5 scenario, there is considerable disagreement between the models as to the projected NPP changes: CSIRO and GISS indicate unchanged or slightly higher NPP during summer and autumn (Figs. 9e,h). This is also the case for IPSL in early summer, though a sharp decline toward the end of the twenty-first century in August is projected (Fig. 9k). The
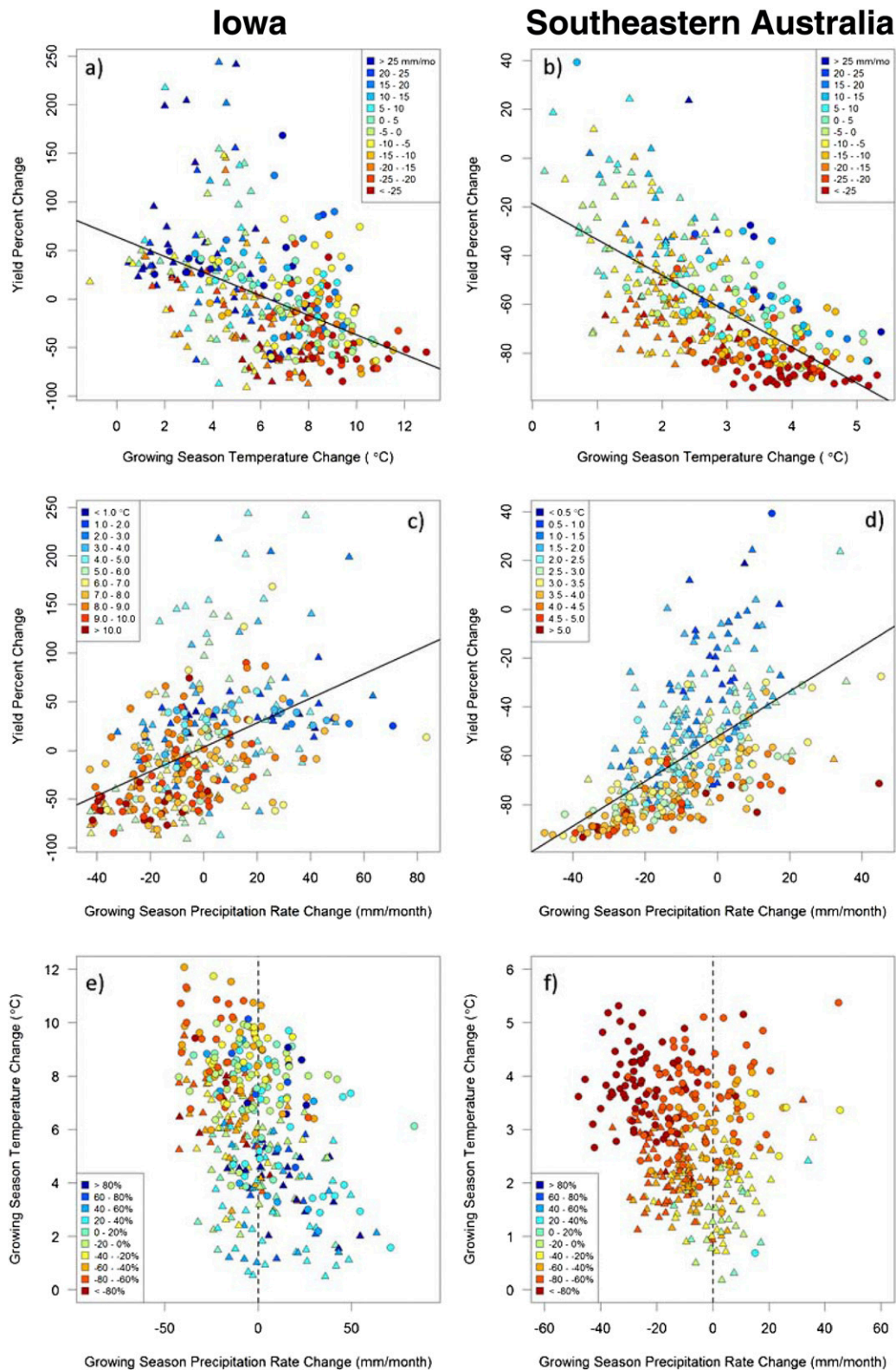
Iowa

Southeastern Australia

FIG. 7. Percentage change of future/projected crop yield in relation to a change in (a),(b) temperature (°C), (c),(d) precipitation (mm month^{-1}), and (e),(f) temperature and precipitation combined for (left) maize in Iowa and (right) wheat in southeastern Australia over the respective growing season. Symbols represent individual years in the period 2071–2100 for each of the six GCMs in the RCP4.5 (triangles) and RCP8.5 (circles) scenarios, relative to a baseline for 1951–80 in the historical scenario.
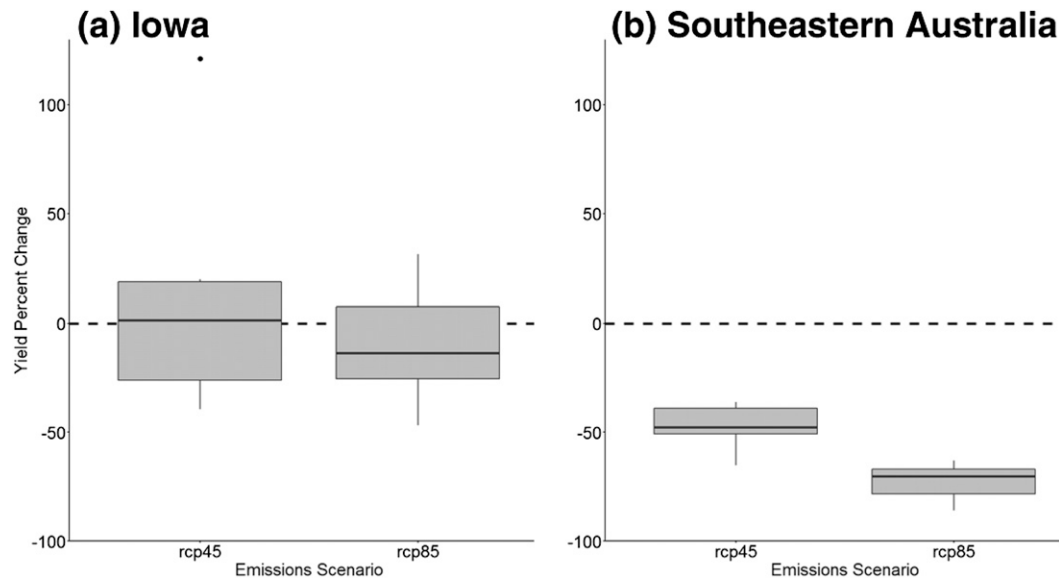
FIG. 8. Range of projected percentage crop-yield changes for (a) Iowa and (b) southeastern Australia, averaged for the period 2071–2100 for the RCP4.5 and RCP8.5 scenarios, relative to a baseline for 1951–80 in the historical scenario for all six GCMs. The box is delimited by the 25th and 75th percentile, with the median indicated as a thick line in between; the whiskers correspond to 1.5 of the interquartile range; and dots correspond to outliers.

NOAA model projects increased NPP in July and August by the 2050s, compared to the start and end of the twenty-first century (Fig. 9t). In contrast, summer and autumn NPP in the MIROC and NCAR models are considerably reduced by the end of the twenty-first century in RCP4.5 (Figs. 9n,q), possibly related to the considerable drop in projected summertime precipitation (for MIROC; Fig. 2).

For the RCP8.5 scenario, shifts in the MMM NPP seasonal cycle over the twenty-first century are apparent: while NPP peaks in July at the start of the twenty-first century, the peak occurs progressively earlier (by June by the end of the twenty-first century; Fig. 9c). Coincident with that shift in the NPP seasonal cycle is a progressive decrease in late summer and autumn NPP toward the end of the twenty-first century. Both the advance in the NPP seasonal cycle and decrease at the end of the growing season by the end of the twenty-first century are consistently seen across models in the RCP8.5 scenario but are especially pronounced in IPSL, MIROC, and NCAR (Figs. 9l,o,r), all models with a pronounced projected summertime drop in precipitation (Figs. 2g,j,m).

b. Southeastern Australia

We also assessed the evolution of the seasonal cycle of NPP for wheat in southeastern Australia in the MMM and individual models for the three scenarios

(Fig. 10). Here, the NPP in the MMM for the historical scenario is 0 from January to June, starts increasing in July, peaks in October, and sharply decreases thereafter with the end of the growing season (Fig. 10a). Most of the models closely agree with regard to the timing of the seasonal cycle of NPP in the historical scenario. An exception is the IPSL model, whose NPP seasonal cycle is shifted forward by two months (Fig. 10j), possibly related to its lack of a well-defined annual cycle in precipitation and overall low winter rainfall (Fig. 4g). Generally, models with higher annual total and wintertime precipitation tend to feature high NPP rates, compared to dry-biased models with low NPP, such as IPSL (cf. Figs. 4, 10). While NPP in the different 20-yr periods does not differ in the MMM for the historical scenario, several models (GISS and IPSL) indicate reduced NPP by the end of the twentieth century compared to earlier periods (Figs. 10g,j).

For the twenty-first century, the MMM NPP in the RCP4.5 scenario is substantially reduced at 62% or less of the historical NPP (Fig. 10b). A progressive decrease in NPP over the course of the twenty-first century is also apparent for the different 20-yr periods. Individual models reflect this progressively lower NPP by the end of the twenty-first century, in particular the CSIRO, MIROC, NCAR, and NOAA models (Figs. 10e,n,q,t). In the RCP8.5 scenario, the progressively lower NPP in the MMM is even more
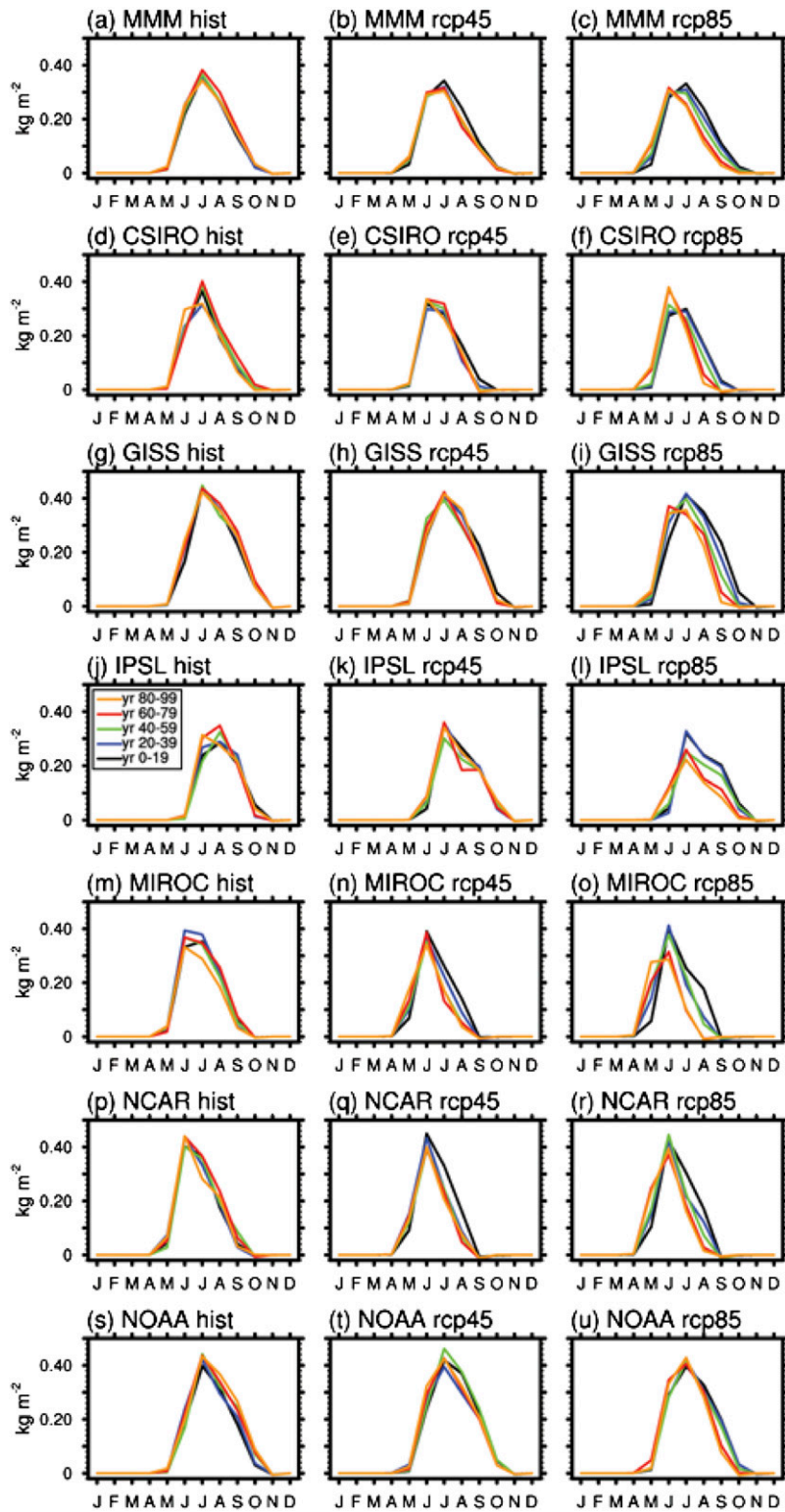
FIG. 9. Seasonal cycle of model total NPP of carbon (kg m^{-2}) for Iowa, shown for the multimodel mean and individual models and scenarios (historical, RCP4.5, and RCP8.5) for different 20-yr periods indicated in color.

FIG. 10. Seasonal cycle of model total NPP of carbon (kg m^{-2}) for southeastern Australia, shown for the multimodel mean and individual models and scenarios (historical, RCP4.5, and RCP8.5) for different 20-yr periods indicated in color.
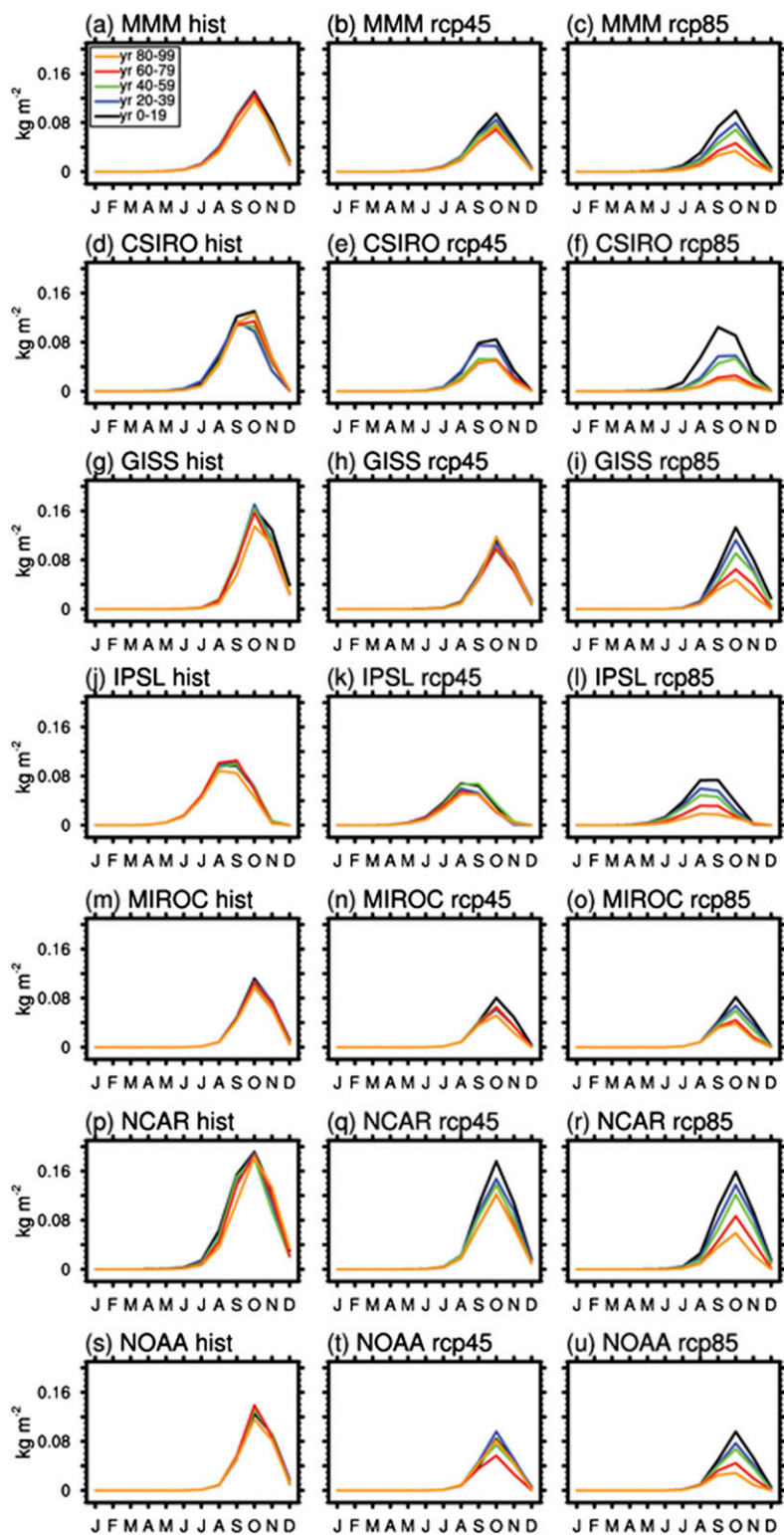
apparent, with NPP by the end of the twenty-first century down to 40% of the rate at the start of the century (Fig. 10c), with results also robust across individual models.

7. Extreme high-/low-yield years

We examined the climate during years recording particularly high/low crop yields in the two regions for the historical and two future emission scenarios. Extreme-yield years were defined using three options, following the approach for maize from Kucharik and Ramankutty (2005), where years exceeding average crop yield by ±8% (option 1), ±20% (option 2), or +6% or −14% (option 3) were defined as extreme.

Time series of simulated annual crop yield (Mg ha^{-1}) for Iowa (Fig. 11) and southeastern Australia (Fig. 12) for the three options show that there is very little difference in the number of extreme years according to options 1 and 3. As per the design, option 2 consistently classifies fewer years as being extreme and a higher number as average (Figs. 11, 12).

For Iowa, the historical average across all models for the three options of extreme years was 34 high- and 35 low-yield years (Fig. 11). This changed only slightly under both RCP4.5 (40 high and 37 low) and RCP8.5 (35 high and 41 low). However, there was substantial variability between climate models in the projection of extreme years both historically (e.g., relatively few extreme years were modeled by GISS, MIROC, and NOAA, as seen in the wide gray bars in Fig. 13) and in the future, where half the climate models predicted an increase in high-yield years (GISS, IPSL, and NOAA), and the other half predicted an increase in low-yield years (CSIRO, MIROC, and NCAR). All climate models predict an increase in extremes (whether more high or low years) by a factor of two or more. Two of the three models projecting more frequent high crop-yield years overall record future increased or sustained levels of summer precipitation in Iowa (cf. Figs. 2d,p), and the third has similar precipitation, except under RCP8.5 (Fig. 2g). In contrast, the models with more low-yield years tend to record decreased summer precipitation, particularly for July and most pronounced in the MIROC model (cf. Fig. 2j).

For southeastern Australia, the amount of interannual variability varies between models, such as low variability for MIROC (Fig. 12j) and higher variability for NOAA (Fig. 12p). However, there is overall much greater intermodel agreement in the number of extreme years for both historical and future scenarios, with an average of 33 high and 34 low crop-yield years, respectively, in the historical scenario across the three extreme-yield

options. In contrast to Iowa, all models show a consistent, dramatic drop in southeast Australian crop yield for the twenty-first century: averaging across the six climate models, only 4 years record a high yield in both future scenarios, while 77 years (RCP4.5) and 83 years (RCP8.5) are classified as low-yield years. For the RCP8.5, half of the models (CSIRO, IPSL, and MIROC) also show a sudden decrease in yield in the second half of the twenty-first century, possibly related to a decrease in cool-season precipitation post-2060 (cf. Fig. 5j).

Since the results did not differ appreciably between the three different options for extreme crop-yield years (not shown), we examined option 2 (i.e., extreme years exceeding average yield by more than ±20%) in more detail to compare differences between climate models and scenarios.

For maize in Iowa, while there was substantial variation between climate models (e.g., GISS predicted only 11 good years under historical conditions, while NCAR predicted 32; the average across all six climate models for option 2 was 24 high-yield years), all models showed similar trends under both future scenarios, with little difference between the RCP4.5 and RCP8.5 scenarios (Fig. 13a). Three models (CSIRO, MIROC, and NCAR) predicted fewer high-yield years and more low-yield years in the future (up to 67 years with low crop yield for MIROC under RCP8.5, retaining only 3 high-yield years). Three models (GISS, IPSL, and NOAA) predicted a reduction in low-yield years and an increase in years with high crop yield in the future; for IPSL, the future projected nearly all years to be high yielding (Fig. 13a).

The projections for wheat in southeastern Australia are more consistent between models, with all models agreeing on a similar distribution of extreme years under the historical scenario, with, on average, 25 high-yield years and, on average, 28 low-yield years (Fig. 13b). In the future, all models agree that, under both scenarios, years with low crop-yield increase in frequency to dominate 66–81 out of the 95 years, with few average years and very few to no high-yield years remaining under both RCP4.5 and RCP8.5 (Fig. 13b). This suggests continued wheat cultivation in southeastern Australia would be extremely difficult under current management practices, and substantial adaptation would be required to continue wheat production there under the future predicted climate.

8. Climate anomalies during high/low crop-yield years

a. Iowa

To evaluate climatic factors potentially contributing to the extremes in crop yield, we show precipitation and
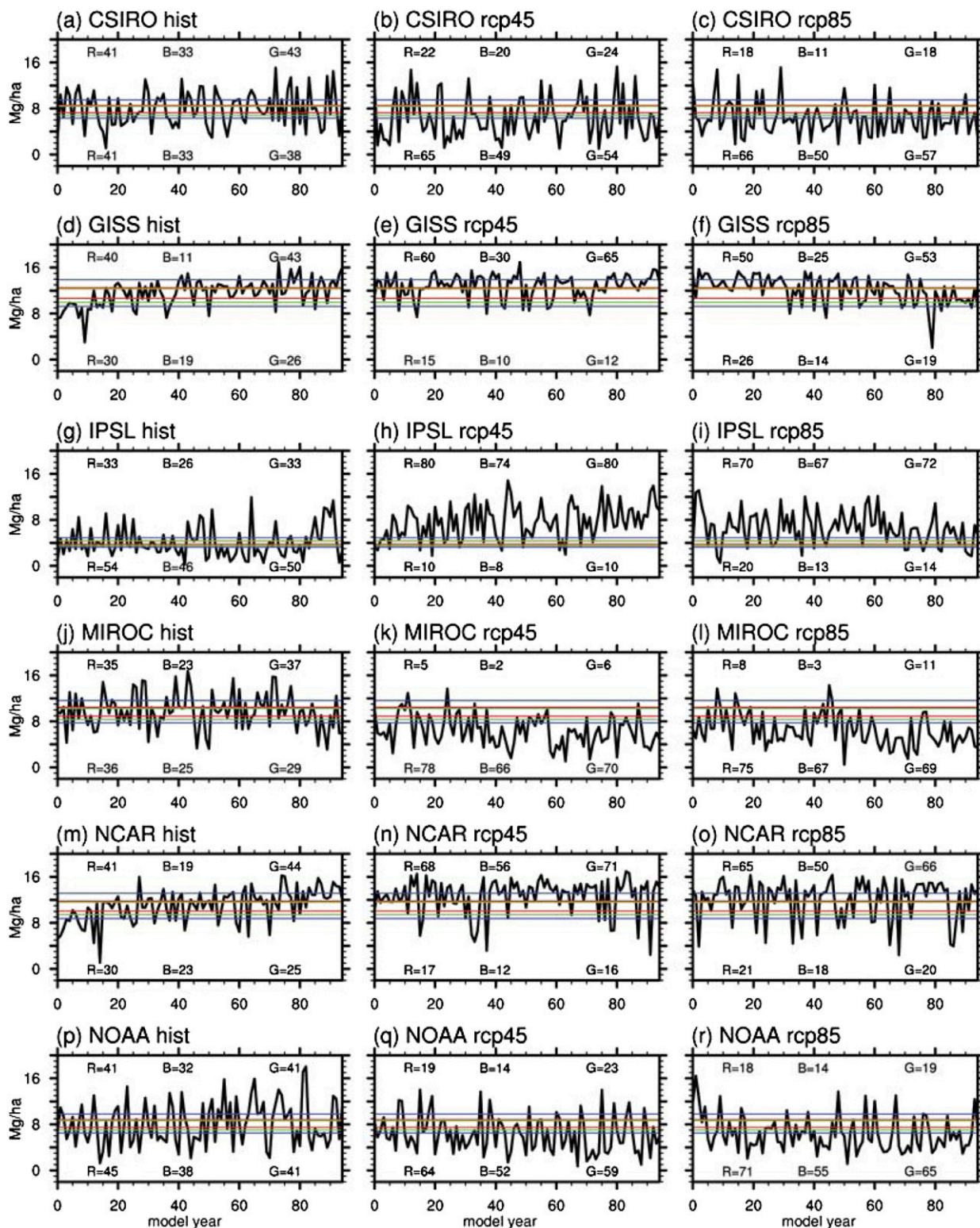
FIG. 11. Model crop yield (Mg ha^{-1}) for Iowa, shown as time series for the different models and scenarios (historical, RCP4.5, and RCP8.5). The horizontal lines indicate the cutoff values for option 1 (R red, extreme years classified as exceeding average by ±8%), option 2 (B blue, exceeding ±20%), and option 3 (G green, exceeding +6% or −14%), with the number of high-/low-yield years selected according to the respective cutoff indicated above/below the time series.
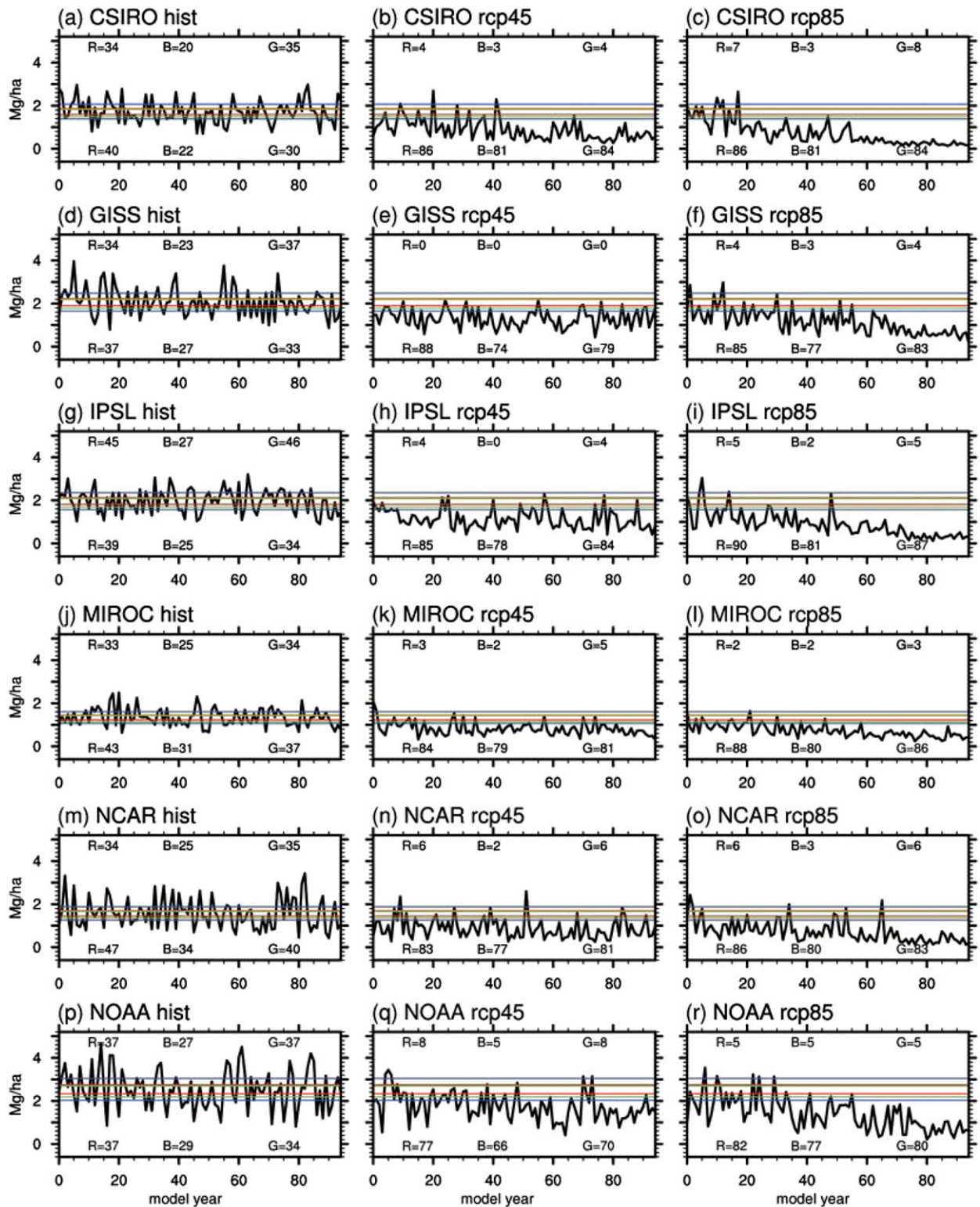
FIG. 12. Model crop yield (Mg ha^{-1}) for southeastern Australia, shown as time series for the different models and scenarios (historical, RCP4.5, and RCP8.5). The horizontal lines indicate the cutoff values for option 1 (R red, extreme years classified as exceeding average by ±8%), option 2 (B blue, exceeding ±20%), and option 3 (G green, exceeding +6% or −14%), with the number of high-/low-yield years selected according to the respective cutoff indicated above/below the time series.
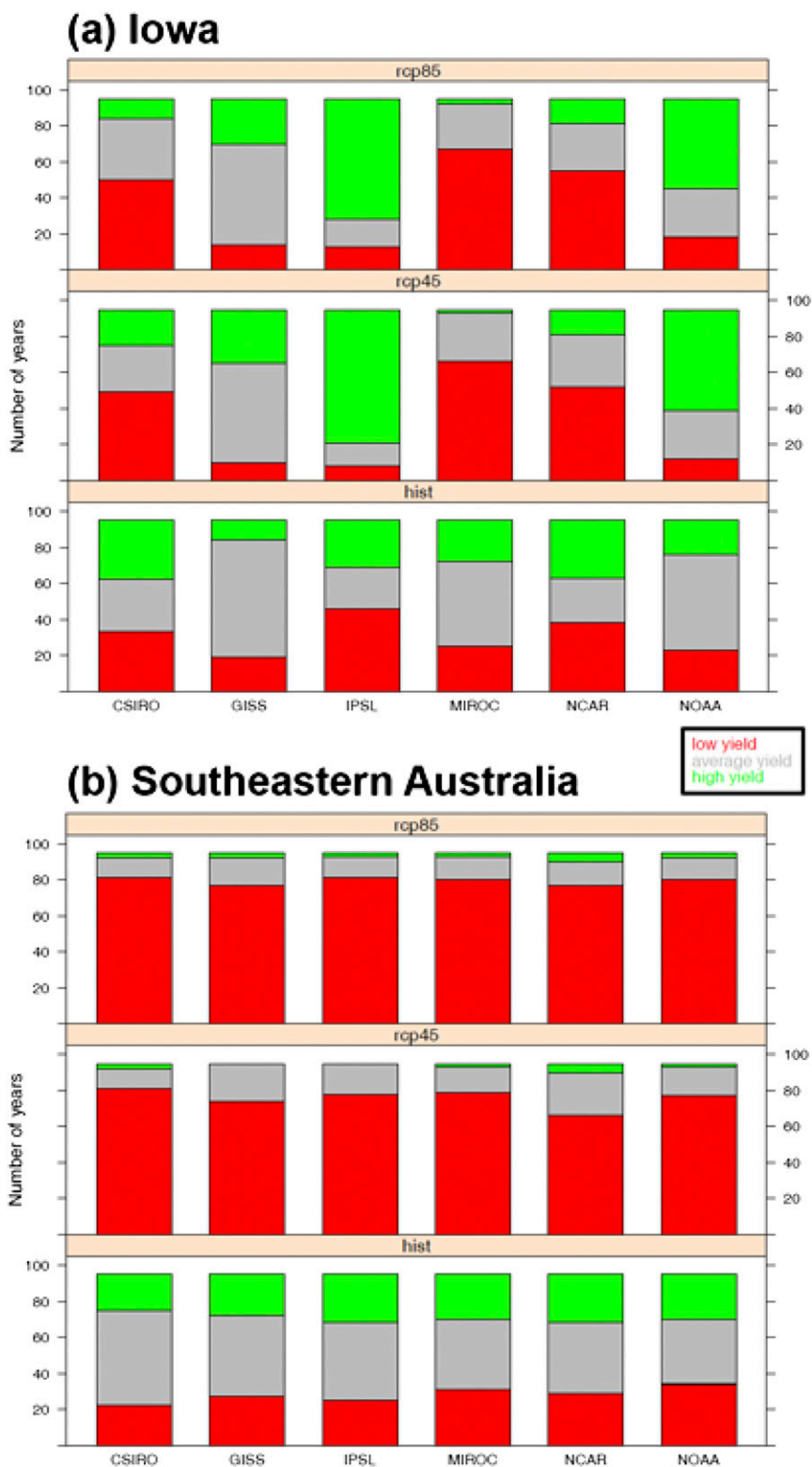
FIG. 13. Number of years of average or extreme yields for the different climate models and scenarios for (a) maize in Iowa and (b) wheat in southeastern Australia. High-yield years are defined as those exceeding the long-term average yield by 20% (green bars), and low-yield years are defined as those with yields 20% below the long-term average (red bars), with average years shown in gray.

temperature anomalies during high and low crop-yield years for Iowa in Figs. 14–16. The mean seasonal cycle of precipitation in Iowa for the six different models and three emissions scenarios is indicated in Fig. 14 during years defined as high and low crop-yield years with the blue and red lines, respectively. To determine whether the mean seasonal cycle during these extreme years differs significantly from average years, a boot-strapping method (i.e., Monte Carlo test) was employed: for a particular scenario and model, the same number of years defined as either having high or low yield were randomly selected from the historical scenario. This was repeated 25 000 times to generate an expected distribution of the seasonal cycle for a given number of years. The blue and red shading in Fig. 14 thus represents the 90% confidence level of this expected distribution for high and low crop-yield years, respectively. Wherever a blue/red line lies outside the blue/red shading, the precipitation in the high-/low-yield years differs significantly from average years. It should be noted that because of differing numbers of high and low crop-yield years, the width of the confidence level indicated by the shading deviates; where shading in only one color is shown, the number of years does not differ, and the shading applies to both high and low crop-yield years (irrespective of its color).

For the historical scenario, most models indicate that years with a low crop yield are characterized by a significant reduction in precipitation during summer: NOAA for July–August (Fig. 14p), MIROC and NCAR for JJA (Figs. 14j,m), and CSIRO for June–September (Fig. 14a); only GISS and IPSL do not record significant deviations in precipitation during low-yield years (Figs. 14d,g). Conversely, high-yield years exhibit anomalous wet conditions during summertime: enhanced precipitation during July in the GISS and NOAA models (Figs. 14d,p), JJA in CSIRO and MIROC (Figs. 14a,j), May–September in NCAR (Fig. 14m), and September only in IPSL (Fig. 14g).

In the twenty-first century for the RCP4.5 emissions scenario, high crop-yield years are characterized in several models by significantly enhanced early-summer precipitation, such as May–July (NCAR and NOAA; Figs. 14n,q) and May–August (CSIRO; Fig. 14b). The GISS model exhibits anomalous wet conditions for much of the first half year (i.e., March–July) during high-yield years and for February–April of low-yield years (Fig. 14e). Years with low crop yield in RCP4.5 exhibit significant reductions in July precipitation, consistent across all models. This reduction in summer precipitation is also apparent during low-yield years in the RCP8.5 scenario, though the decrease often extends beyond the month of July. Overall, fewer high-yield

years are seen for Iowa in the RCP8.5 (relative to RCP4.5), but the anomalous high precipitation is more extensive: above-average precipitation occurs for much of the year for the CSIRO, GISS, NCAR, and NOAA models (Figs. 14c,f,o,r) during years with high crop yield in Iowa in RCP8.5.

Temperature anomalies have also been shown to influence variations in maize yield, with negative effects on future maize yield projected because of rising temperatures (e.g., Schlenker and Roberts 2009; Lobell et al. 2011a; Butler and Huybers 2013; Lobell et al. 2013). Given the seasonal dependence of the susceptibility of plants during specific physiological stages to temperature stress (Sanchez et al. 2014), we thus show the seasonal cycle of $T_{\min}$ and $T_{\max}$ in Iowa during high and low crop-yield years for the CSIRO and MIROC models for the three emissions scenarios in Fig. 15. The CSIRO and MIROC models were chosen as a result of the large magnitude of the projected increase in $T_{\min}$ and $T_{\max}$ in Iowa in the twenty-first century (Figs. 2b,c,k,l), with the summertime rise in $T_{\max}$ in MIROC largest of all the models analyzed here. Significance levels were determined as for precipitation in Fig. 14. The $T_{\min}$ during high and low crop-yield years in the historical simulation only deviated slightly from average years during July and August for both models (Figs. 15a,d). In the twenty-first century, $T_{\min}$ in both models is significantly higher than present average conditions throughout the year in low crop-yield years, but especially during June–September for both emissions scenarios, and also for January–February in RCP8.5 (Figs. 15b,c,e,f). While warmer $T_{\min}$ throughout the year in the twenty-first century also characterize high-yield years in the CSIRO model (Figs. 15b,c), significantly warmer temperatures in MIROC are only seen in the RCP8.5 scenario (Fig. 15f): it seems that $T_{\min}$ in RCP4.5 in MIROC during high-yield years does not differ significantly from average historical conditions, but it does for RCP8.5; it should be noted that the small number of high-yield years in MIROC in the twenty-first century and the resultant width of the expected distribution could play a role in this result.

The $T_{\max}$ are significantly increased during low crop-yield years in Iowa in the historical simulation, while $T_{\max}$ does not deviate significantly from average conditions during high-yield years (Figs. 15g,j). While both high and low crop-yield years in the twenty-first century are characterized by significantly warmer $T_{\max}$ for much of the year than during historical average years (Figs. 15h,i,k,l), this is especially pronounced during low-yield years: Iowa summertime $T_{\max}$ exceeds historical levels by 5°C or more, particularly in July and August, for both models. In contrast, high-yield years in summertime in RCP4.5 do
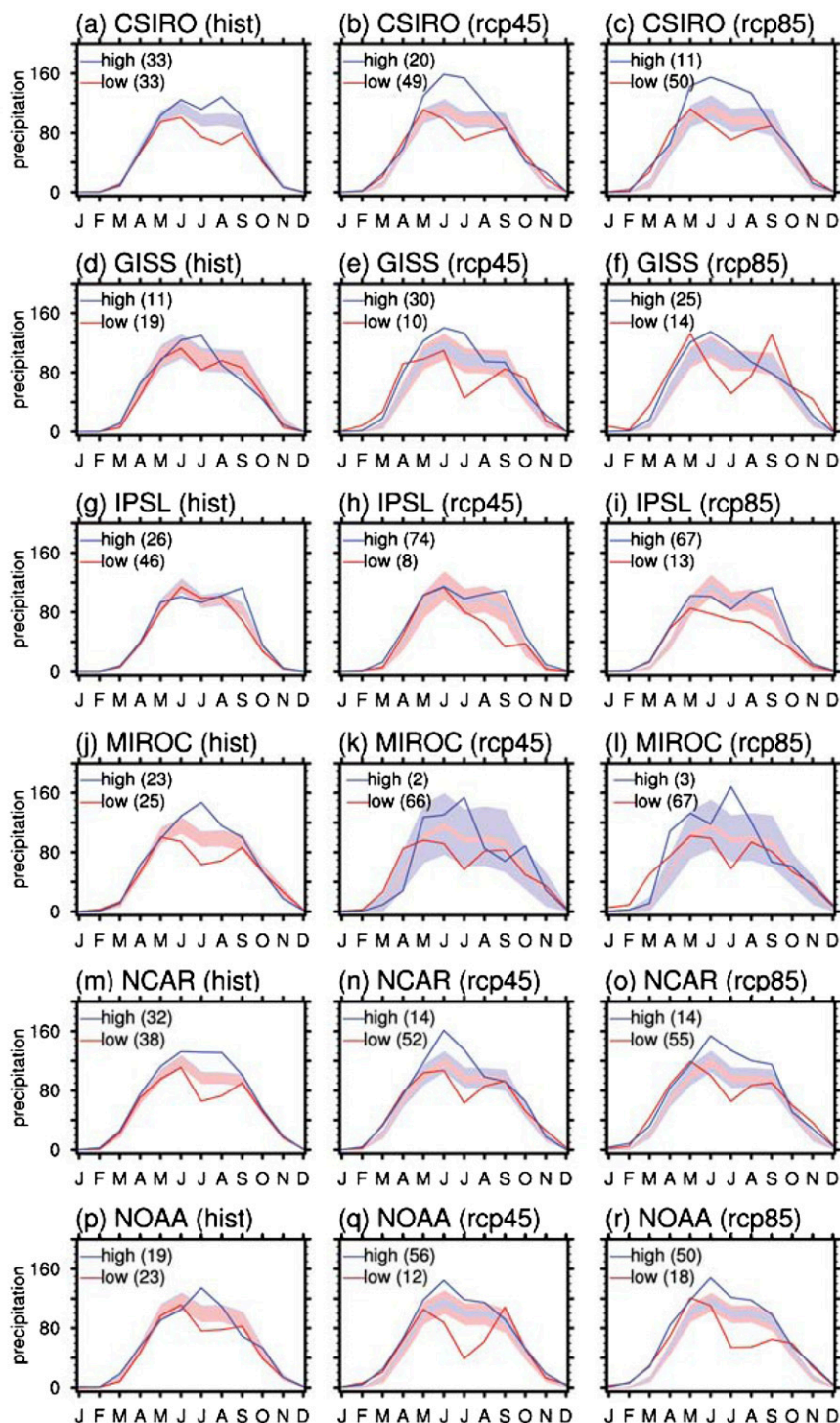
FIG. 14. Seasonal cycle of precipitation (mm month^{-1}) during years with high (blue) and low (red) crop yield (according to yields exceeding ±20% of average, as in option 2 in Fig. 11) for Iowa, shown for the three scenarios (historical, RCP4.5, and RCP8.5) across the different models. Shading indicates the 90% confidence level around an average seasonal cycle for the respective number of extreme years in the scenario and model, as determined by Monte Carlo testing. Where the red (blue) line lies outside the shaded area, the values are significantly different from the average seasonal cycle in the historical scenario.
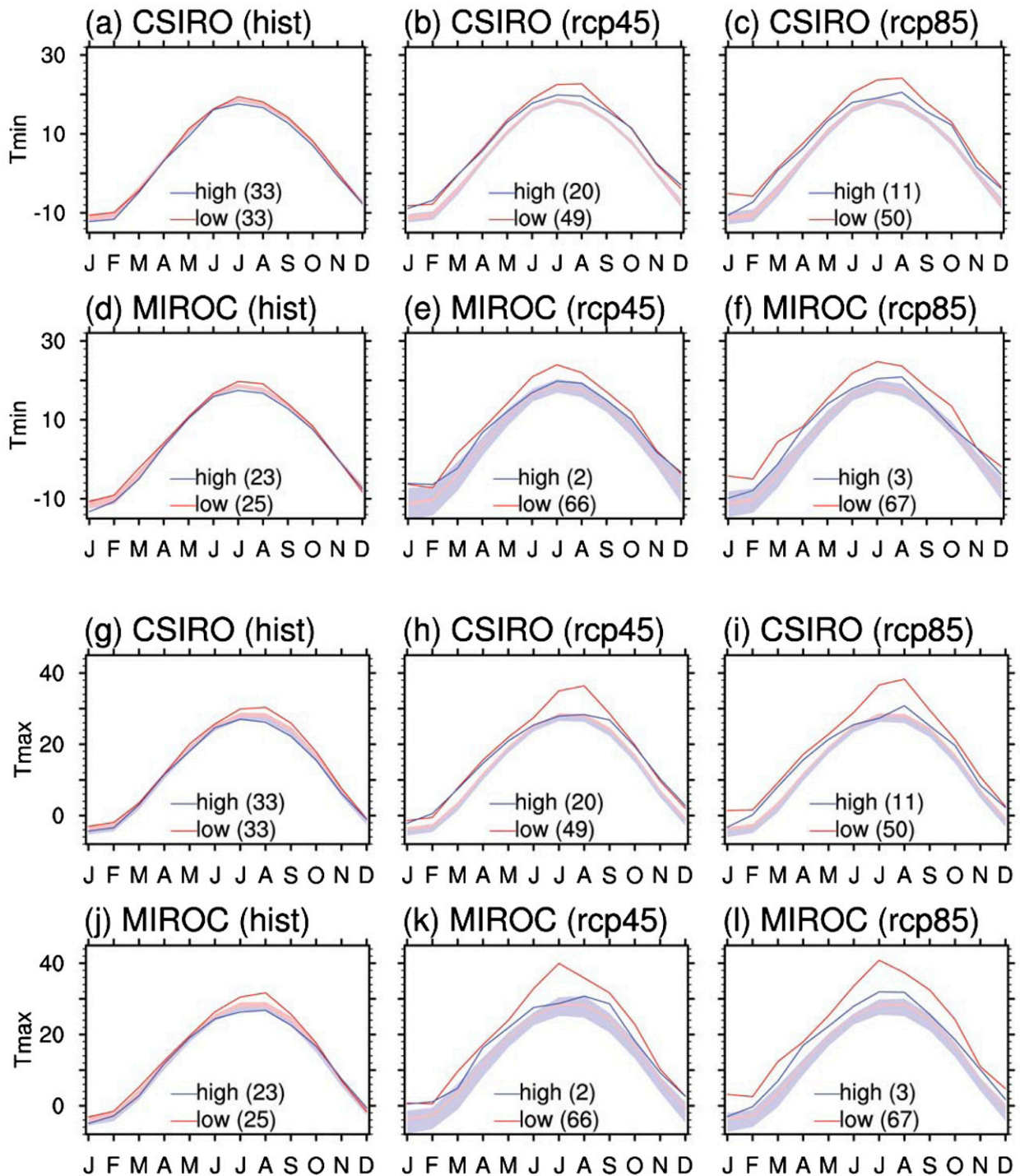
FIG. 15. Seasonal cycle of T_{min} and T_{max} (°C) during years with high (blue) and low (red) crop yield (according to yields exceeding ±20% of average, as in option 2 in Fig. 11) for Iowa, shown for the three scenarios (historical, RCP4.5, and RCP8.5) across the different models. Shading indicates the 90% confidence level around an average seasonal cycle for the respective number of extreme years in the scenario and model, as determined by Monte Carlo testing. Where the red (blue) line lies outside the shaded area, the values are significantly different from the average seasonal cycle in the historical scenario.
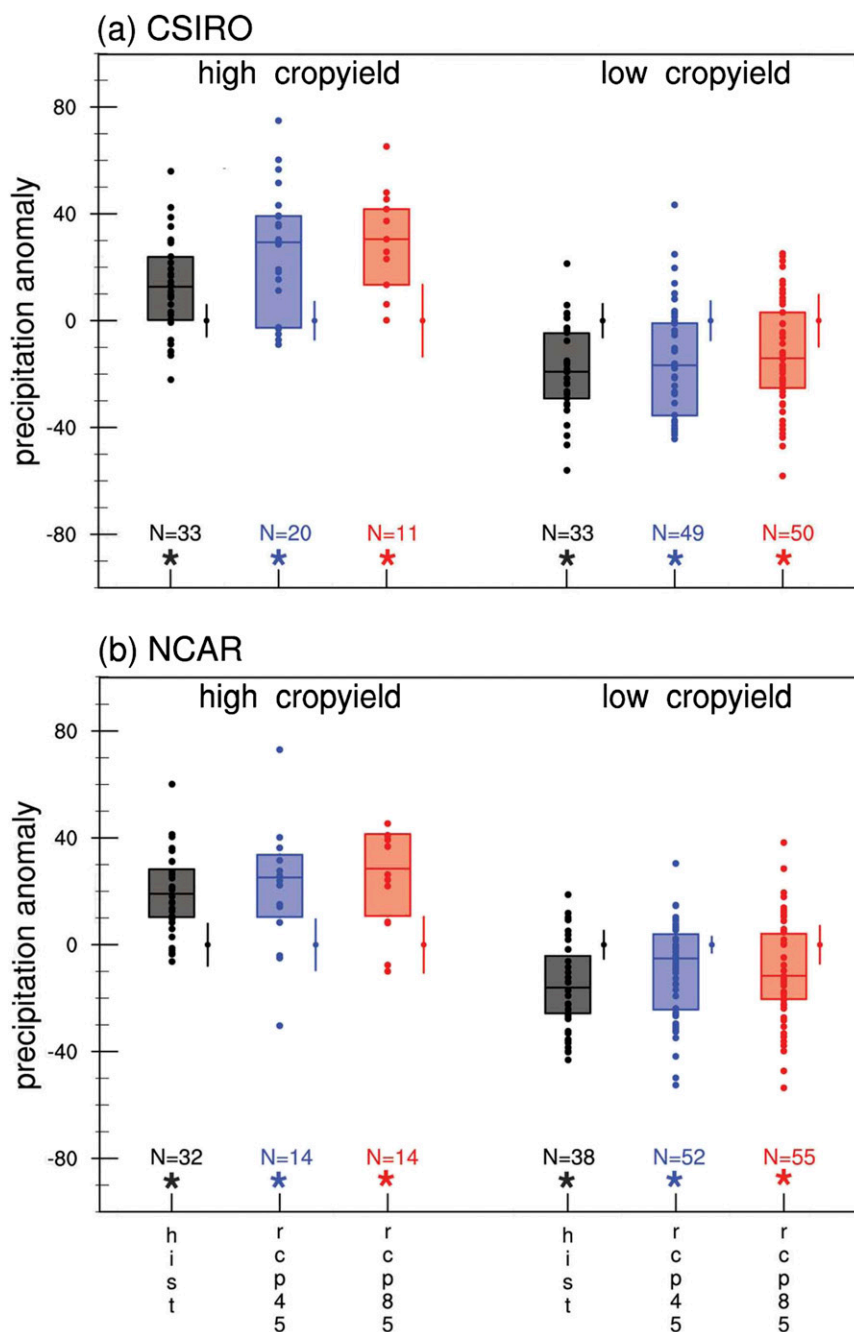
FIG. 16. Average May–September Iowa precipitation anomaly (mm month^{-1}) for the three scenarios during high/low crop-yield years for the (a) CSIRO and (b) NCAR model, shown as dots for the individual years. The colored boxes are delimited by the upper and lower quartiles, with the middle bar denoting the median precipitation anomaly for the respective scenario: historical (black), RCP4.5 (blue), and RCP8.5 (red). Error bars indicate the value the median needs to exceed to be significantly different from 0 (at the 90% confidence level, as estimated by Monte Carlo testing) for the different scenarios, with asterisks indicating significance. The number *N* indicates the number of years exceeding the cutoff crop yield for each scenario. Wherever the median precipitation anomalies during high and low years do not overlap with the error bar, precipitation during the extreme years differs significantly from average historical conditions.

not show significantly warmer T_{max} compared to historical average conditions, but they do for the first half of the year (Figs. 15h,k). Given the negative effect of T_{max} on maize yield (Lobell et al. 2011a, 2013; Sanchez et al. 2014), which we also see for low-yield years, the more moderate T_{max} in high-yield years could contribute to the higher yields recorded.

Given the distinct seasonal cycle in precipitation during high and low crop-yield years in Iowa identified here (cf. Fig. 14), it is of interest to further investigate precipitation anomalies during extreme years. Figure 16 shows Iowa precipitation anomalies averaged over the May–September months during the maize growing season during high and low crop-yield years for the three scenarios for the CSIRO and NCAR model. Both the CSIRO and NCAR models show a robust precipitation response during extreme years in the historical scenario (Figs. 14a,m), while maintaining sufficient extreme years in the twenty-first century to explore precipitation anomalies during these years in the twenty-first century (unlike, for example, the MIROC model, which also exhibits significant precipitation anomalies in the twentieth century but has only a few years with extreme high yield in the twenty-first century; Figs. 14j–l).

For the CSIRO model, it is apparent that years with high crop yield are characterized by significantly enhanced May–September precipitation in Iowa compared to average years (Fig. 16a). While median precipitation anomalies in the historical scenario are on the order of 15 mm month^{-1}, this increases to 30 mm month^{-1} in the RCP4.5 and RCP8.5 scenarios for high-yield years. Low crop-yield years in the CSIRO model exhibit significant reductions in precipitation on the order of -20 mm month^{-1} for historical and future scenarios alike (Fig. 16a). For the NCAR model, high crop-yield years are characterized by significantly enhanced May–September median precipitation anomalies, on the order of $+20$, $+25$, and $+30$ mm month^{-1} for the historical, RCP4.5, and RCP8.5 scenarios, respectively (Fig. 16b). In contrast, low crop-yield years are characterized by substantial decreases in median precipitation of -15 (historical), -5 (RCP4.5), and -10 mm month^{-1} (RCP8.5; Fig. 16b).

b. Southeastern Australia

Climate anomalies during extreme crop-yield years in southeastern Australia are shown in Figs. 17–19. In the historical scenario, there is a tendency across several models for high (low) crop-yield years to be associated with significantly wetter (drier) conditions during austral spring compared to average years (Figs. 17a,d,j,m,p), especially pronounced in the NOAA model for the August–November months (Fig. 17p). The very small number of high crop-yield years in the twenty-first century makes it

difficult to determine statistically robust results for deviations in the seasonal cycle of precipitation for these years. In contrast, the large number of low-yield years in the twenty-first century in RCP4.5 and RCP8.5 are characterized by anomalous low precipitation compared to historical conditions for most of the year, but in particular for austral spring (Fig. 17).

For the most part, the seasonal cycle of minimum and maximum temperature for the CSIRO and MIROC models indicate that extreme crop-yield years do not significantly deviate from average historical conditions in the twentieth century in southeastern Australia (Fig. 18). One exception is warmer (colder) T_{max} conditions during austral spring for low (high) crop-yield years, respectively (Figs. 18g,j). For the twenty-first century, no significant deviations are seen in the seasonal cycle for T_{min} or T_{max} during years with high crop yield. In contrast, low crop-yield years are characterized by significantly warmer T_{min} and T_{max} values for most of the year for both models in RCP4.5 and even more so for RCP8.5. This is consistent with previous work documenting that extreme high temperatures adversely affect wheat yields (e.g., Nicholls 1997; Porter and Gawith 1999; Wang et al. 2011). Again, for the interpretation of these results, one has to be mindful of the disparity in the number of future high and low crop-yield years.

Examples of southeastern Australian precipitation anomalies during the growing season (June–October) for extreme crop-yield years are provided for the CSIRO and NOAA models (Fig. 19), which exhibit significant deviations in springtime precipitation for high- and low-yield years during historical conditions (Figs. 17a,p). In both models, high crop yield is associated with anomalous wet conditions, both in the historical scenario and even more so during the few high-yield years in the twenty-first century. While median precipitation anomalies on the order of $+12$ mm month^{-1} occur during high-yield years under historical conditions, the median anomaly in RCP4.5 is approximately $+25$ and $+27$ mm month^{-1} for RCP8.5 for the NOAA model (Fig. 19b). In the CSIRO model, growing season rainfall during low-yield years does not deviate significantly from average conditions in the historical scenario; in the twenty-first century, however, significant reductions in precipitation occur during low-yield years in southeastern Australia for both RCP4.5 and RCP8.5 (Fig. 19a). In the NOAA model, years with low crop yield are characterized by anomalous dry conditions in all three scenarios (Fig. 19b).

9. Summary

We used multiple CMIP5 climate models and scenarios to assess historical and future hydroclimatic
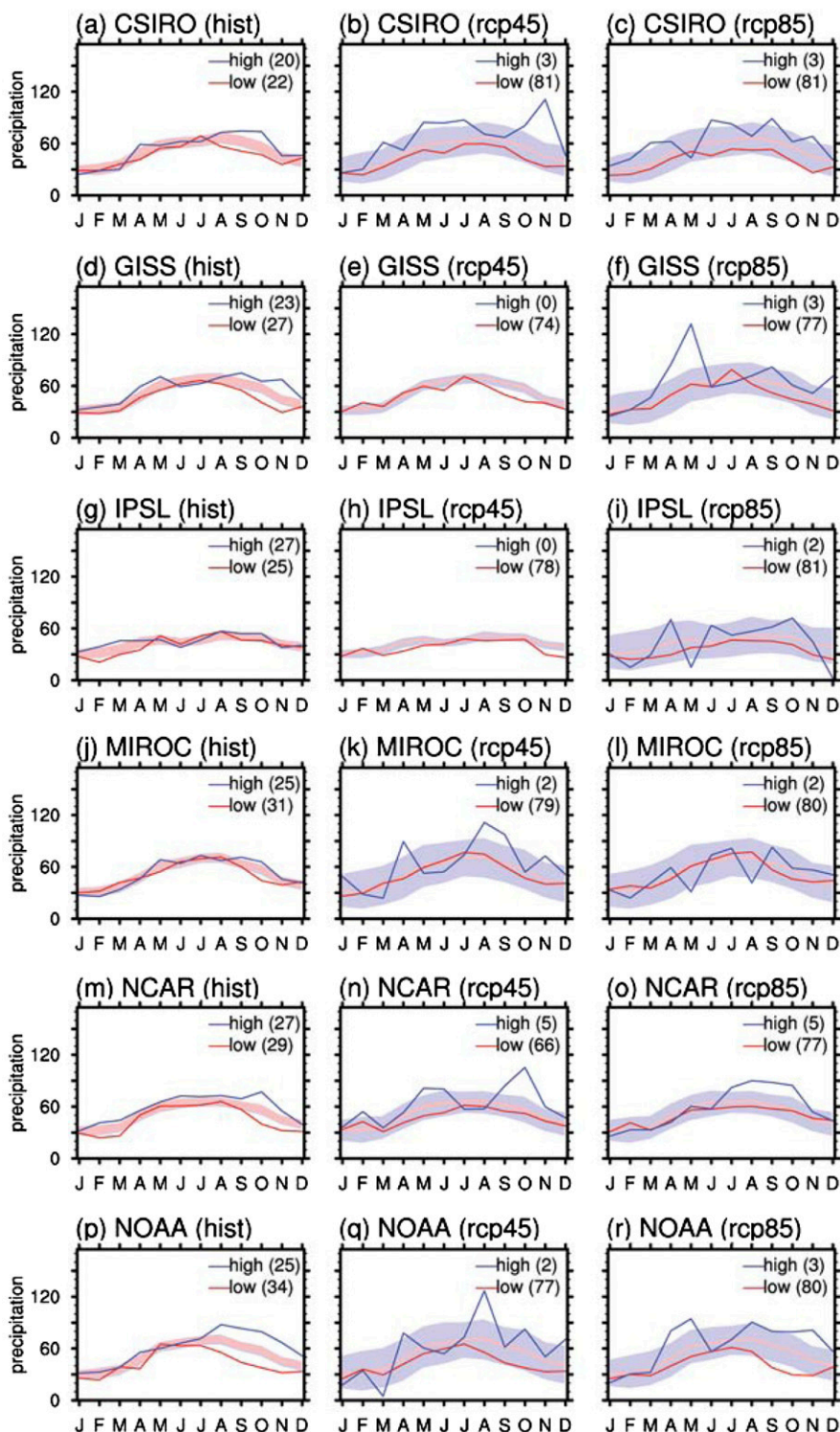
FIG. 17. Seasonal cycle of precipitation (mm month^{-1}) during years with high (blue) and low (red) crop yield (according to yields exceeding +/−20% of average, as in option 2 in Fig. 12) for southeastern Australia, shown for the three scenarios (historical, RCP4.5, and RCP8.5) across the different models. Shading indicates the 90% confidence level around an average seasonal cycle for the respective number of extreme years in the scenario and model, as determined by Monte Carlo testing. Where the red (blue) line lies outside the shaded area, the values are significantly different from the average seasonal cycle in the historical scenario.
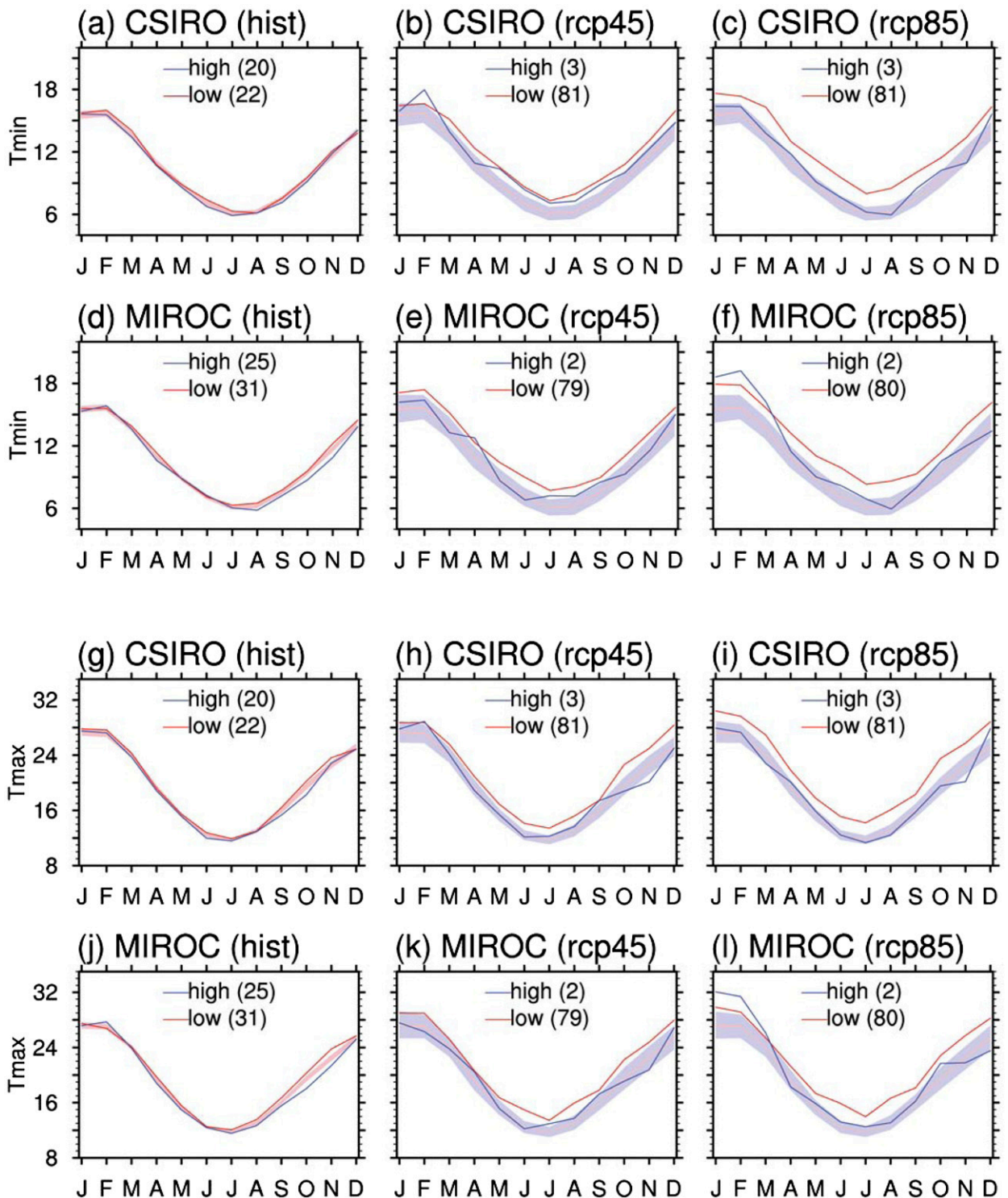
FIG. 18. Seasonal cycle of T_{min} and T_{max} (°C) during years with high (blue) and low (red) crop yield (according to yields exceeding +/−20% of average, as in option 2 in Fig. 12) for southeastern Australia, shown for the three scenarios (historical, RCP4.5 and RCP8.5) across the different models. Shading indicates the 90% confidence level around an average seasonal cycle for the respective number of extreme years in the scenario and model, as determined by Monte Carlo testing. Where the red (blue) line lies outside the shaded area, the values are significantly different from the average seasonal cycle in the historical scenario.
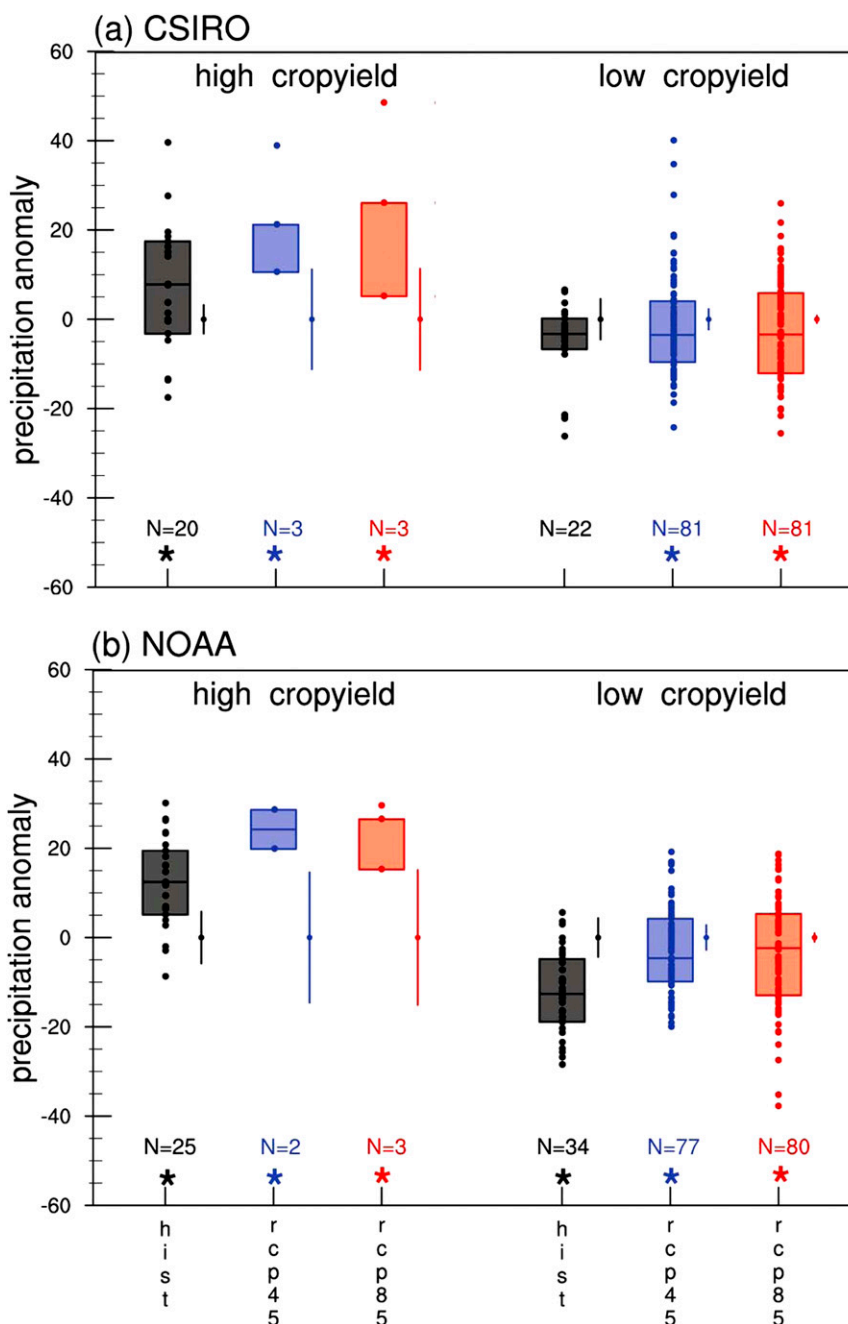
FIG. 19. Average June–October southeastern Australian precipitation anomaly (mm month^{-1}) for the three scenarios during high/low crop-yield years for the (a) CSIRO and (b) NOAA model, shown as dots for the individual years. The colored boxes are delimited by the upper and lower quartiles, with the middle bar denoting the median precipitation anomaly for the respective scenario: historical (black), RCP4.5 (blue), and RCP8.5 (red). Error bars indicate the value the median needs to exceed to be significantly different from 0 (at the 90% confidence level, as estimated by Monte Carlo testing) for the different scenarios, with asterisks indicating significance. The number *N* indicates the number of years exceeding the cutoff crop yield for each scenario. Wherever the median precipitation anomalies during high and low years do not overlap with the error bar, precipitation during the extreme years differs significantly from average historical conditions.

TABLE 2. Changes in growing season precipitation, T_{min}, T_{max}, and yield in Iowa and southeastern Australia in the RCP4.5 and RCP8.5 scenarios relative to historical conditions, averaged over the last 30 years in each scenario for six GCMs and the multimodel mean. The growing season in Iowa (southeastern Australia) is May–September (June–October).

	Model	Scenario	Precipitation	T_{min}	T_{max}	Yield
				Changes in		
Iowa	CSIRO	RCP4.5	+7%	+4.3°C	+4.4°C	−18%
		RCP8.5	+5%	+7.4°C	+8.2°C	−27%
	GISS	RCP4.5	+4%	+3.1°C	+6.2°C	+1%
		RCP8.5	−2%	+5.8°C	+10.3°C	−17%
	IPSL	RCP4.5	+13%	+3.7°C	+5.4°C	+106%
		RCP8.5	−8%	+6.8°C	+11.2°C	+23%
	MIROC	RCP4.5	−15%	+5.2°C	+9.4°C	−38%
		RCP8.5	−16%	+8.0°C	+12.5°C	−46%
	NCAR	RCP4.5	−6%	+4.0°C	+6.0°C	−37%
		RCP8.5	−11%	+5.8°C	+9.3°C	−33%
	NOAA	RCP4.5	+3%	+1.2°C	+1.7°C	0%
		RCP8.5	+6%	+4.2°C	+5.2°C	−6%
	MMM	RCP4.5	+1%	+3.6°C	+5.5°C	+8%
		RCP8.5	−4%	+6.3°C	+9.5°C	−18%
Australia	CSIRO	RCP4.5	−19%	+2.0°C	+2.8°C	−65%
		RCP8.5	−32%	+3.3°C	+4.7°C	−86%
	GISS	RCP4.5	0%	+1.3°C	+2.2°C	−29%
		RCP8.5	−6%	+2.8°C	+4.3°C	−64%
	IPSL	RCP4.5	−9%	+0.7°C	+2.5°C	−47%
		RCP8.5	−20%	+1.6°C	+4.8°C	−79%
	MIROC	RCP4.5	+6%	+2.0°C	+2.9°C	−43%
		RCP8.5	+4%	+3.1°C	+4.2°C	−61%
	NCAR	RCP4.5	−5%	+1.7°C	+3.1°C	−35%
		RCP8.5	−2%	+3.2°C	+5.4°C	−66%
	NOAA	RCP4.5	−15%	+1.3°C	+2.3°C	−47%
		RCP8.5	−31%	+2.7°C	+3.8°C	−72%
	MMM	RCP4.5	−7%	+1.5°C	+2.6°C	−44%
		RCP8.5	−15%	+2.8°C	+4.5°C	−71%

conditions and their effect on maize yield in Iowa and wheat in southeast Australia. The agreement between simulated maize (wheat) yield in Agro-IBIS and observed yields in Iowa (southeastern Australia) attests the model's effectiveness to assess the impact of climate variability and change on crop yield. Beyond mean changes in precipitation, T_{min}, and T_{max}, emphasis was placed on changes in year-to-year variability in these variables, seasonal changes during sensitive phases in crop growth, and climatic conditions during years with extreme crop yield.

For Iowa, precipitation changes are small in the RCP4.5 scenario, but in RCP8.5, spring precipitation in the twenty-first century is projected to increase across models, while some also indicate a slight reduction in summer precipitation (Figs. 2, 3), resulting in negligible overall growing season precipitation change for Iowa in the MMM (Table 2). Warmer temperatures, especially in summer and winter for T_{min} and summer for T_{max}, are projected to occur across the models (Fig. 2), with growing season temperature changes in the MMM on the order of +3.6° to +5.5°C (+6.3° to +9.5°C) by the

end of the twenty-first century for RCP4.5 (RCP8.5) (Table 2). While changes in Iowa maize yield by the end of the twenty-first century are small in RCP4.5 (+8%), reductions on the order of −20% are projected in RCP8.5 (Fig. 8, Table 2). In the historical scenario, the number of high-, low-, and average-yield years in Iowa is comparable across models at a third each. For the twenty-first century, the three models recording increased or sustained summer precipitation project more frequent high-yield years and fewer years with low crop yield (Figs. 2, 11). In contrast, the three models projecting decreased Iowa summer precipitation indicate fewer high-yield years and more frequent low-yield years. In the twenty-first century, high crop-yield years record significantly enhanced early-summer precipitation, while low-yield years are characterized by significant reductions in summer precipitation and anomalously high T_{max} (Figs. 14–16), both likely factors contributing to the reduced yield in these years.

In southeastern Australia, the projections indicate a reduction in precipitation in the twenty-first century, especially pronounced in spring and in late autumn

(April–June) in the RCP8.5 scenario (Figs. 4, 5j), resulting in a decrease in growing season rainfall in the MMM of −7% (−15%) by the end of the twenty-first century in the RCP4.5 (RCP8.5) scenario (Table 2). MMM growing season temperatures are expected to increase by +1.5° to +2.6°C (+2.8° to +4.5°C) for the RCP4.5 (RCP8.5) scenario (Table 2). Given the increasingly drier and warmer growing season conditions, wheat yield in southeastern Australia is projected to decrease on the order of −50% to −70% by the end of the twenty-first century for RCP4.5 and RCP8.5, respectively (Fig. 8, Table 2). While the yield decreases projected here for wheat in Australia are on the high end, they do not appear to be out of the range of likely scenarios. In their review summarizing results from several previous studies, Wheeler and von Braun (2013) recorded average-yield losses of 20% for southeastern Australia by 2050 for a range of emissions scenarios. Challinor et al. (2010) simulated an upper range of crop failure rates for wheat in China without adaptation above 50% with an increase in local mean temperature between 4°–6°C. Rather than focusing on crop failure, Asseng et al. (2011) modeled wheat yields in Australia directly, finding reductions in grain production of up to 50% with temperature increases of 2°C, mostly attributed to temperatures above 34°C. A meta-analysis conducted two decades ago showed that wheat yields in Australia and the United States were already reduced 10%–15% by temperatures above the optimum during the sensitive stages of anthesis and grain filling and that temperatures in Australia routinely reached between 30°–40°C during grain filling (Wardlaw and Wright 1994). An experiment applying a 40°C heat stress treatment around anthesis produced-yield decreases of 50% (Ferris et al. 1998). A recent analysis concluded that existing models likely underestimate yield losses for +2°C by up to 50% in India by neglecting to account for the effects of extreme heat on wheat senescence (Lobell et al. 2012).

Our results found that, while maize in Iowa can experience yield increases across many of the temperature and precipitation changes projected in the future (Fig. 7e), wheat in southeastern Australia is poised much closer to a biophysical threshold where future changes are nearly all negative (Fig. 7f). Yields in different growing areas may be limited by different combinations of biophysical factors, and further analysis is needed to examine how temperature and precipitation changes are projected to vary in major global growing areas to determine how this would affect crop yields regionally.

The number of high- and low-yield years, which in the historical scenario is consistent across models at a third each, changes dramatically in the twenty-first century: the number of high-yield years drops to less than 10%, while in excess of 60%–80% of years are low yielding (Figs. 12, 13). In the historical scenario, high (low) crop-yield years are associated with significantly wetter (drier) conditions during austral spring compared to average years, which becomes more pronounced for extreme-yield years in future (Figs. 14–19). Significant decreases in growing season rainfall by the end of the twenty-first century in southeastern Australia clearly influence wheat yields, as do higher maximum temperatures in the RCP8.5 scenario during low-yielding years.

This study simulated the effects of temperature and precipitation on crop yields, finding decreases in yields projected. Actual yield losses may be partly offset by projected increases in CO_2, which have been found to increase yields in C3 crops such as wheat, and to a lesser extent C4 crops such as maize, particularly under moisture stress (Ainsworth and Long 2005; Leakey et al. 2006; Lobell and Field 2008; McGrath and Lobell 2011). For example, the CO_2 increase over the past 50 years has been estimated to increase U.S. maize yields by 9% in dry years (McGrath and Lobell 2011). Future work could make more realistic estimates of yields using new parameters in IBIS to model the effects of both CO_2 and ozone on crop yields (Twine et al. 2013).

Our results highlight that projections of future crop yield are highly sensitive to the nature of hydroclimatic changes. Where future hydroclimatic changes are uncertain, as for example for precipitation in Iowa, where half the GCMs project an increase and half a decrease of growing season rainfall, the sign of the crop-yield change simulated by the dynamic vegetation model is uncertain as well. In contrast, broad agreement in projected drying over southern Australia across GCMs is reflected in consistent crop-yield decreases for the twenty-first century. Better understanding of projected changes in mean conditions, seasonal cycle, and in particular variability, along with the associated uncertainties across models and time scales in GCMs, is warranted for improved projections of yields of various staple grains. Our results suggest that managers planning for climate adaptation should focus on adaptation measures that address precipitation decreases that will challenge conditions for wheat growing in Australia and precipitation decreases and increased temperatures in Iowa, but further examination of these measures is needed.

Climate Model Diagnosis and Intercomparison (PCMDI) provided coordinating support and led development of software infrastructure in partnership with the Global Organization for Earth System Science Portals. Use of the following datasets is gratefully acknowledged: precipitation dataset by Dr. Mike Hulme (Climatic Research Unit, University of East Anglia, Norwich, United Kingdom), supported by the U.K. Department of the Environment, Transport and Regions; temperature from the Twentieth Century Reanalysis Project supported by the U.S. DOE, Office of Science Innovative and Novel Computational Impact on Theory and Experiment program and Office of Biological and Environmental Research, and by the National Oceanic and Atmospheric Administration Climate Program Office. This work was initiated at the Dissertations Initiative for the Advancement of Climate Change Research (DISCCRS) V Symposium, supported by the U.S. National Science Foundation through collaborative Grants SES-0932916 and SES-0931402. CCU was supported by a University of New South Wales Vice-Chancellor Fellowship and the Penzance Endowed Fund and John P. Chase Memorial Endowed Fund at WHOI. TET was supported by the U.S. Department of Energy Award DE-EE0004397. NC was funded by NSF Grant EAR-1204774. We are indebted to the FORMAS-funded Land Use Today and Tomorrow (LUsTT) project (Grant 211-2009-1682) for financial support.

REFERENCES

ABARE, 2007: Australian crop report. Australian Bureau of Agricultural and Resource Economics Tech. Rep. 141, 19 pp. [Available online at http://data.daff.gov.au/data/warehouse/pe_abare99001345/acr07.1.pdf.]

——, 2013: Australian crop report. Australian Bureau of Agricultural and Resource Economics Tech. Rep. 168, 21 pp. [Available online at http://data.daff.gov.au/data/warehouse/aucrpd9abcc003/aucrpd9abcc003201306/AustCropReport20130612_v1.0.0.pdf.]

Ainsworth, E. A., and S. P. Long, 2005: What have we learned from 15 years of free-air CO_2 enrichment (FACE)? A meta-analytic review of the responses of photosynthesis, canopy properties and plant production to rising CO_2. *New Phytol.,* **165,** 351–372, doi:10.1111/j.1469-8137.2004.01224.x.

Anderson-Teixeira, K. J., P. K. Snyder, T. E. Twine, S. V. Cuadra, M. H. Costa, and E. H. DeLucia, 2012: Climate-regulation services of natural and agricultural ecoregions of the Americas. *Nat. Climate Change,* **2,** 177–181, doi:10.1038/nclimate1346.

Andresen, J., S. Hilberg, and K. Kunkel, 2012: Historical climate and climate trends in the midwestern USA. Great Lakes Integrated Sciences and Assessment Tech. Rep., 18 pp. [Available online at http://glisa.umich.edu/media/files/NCA/MTIT_Historical.pdf.]

Arnell, N. W., and Coauthors, 2002: The consequences of CO_2 stabilisation for the impacts of climate change. *Climatic Change,* **53,** 413–446, doi:10.1023/A:1015277014327.

Asner, G. P., A. J. Elmore, L. P. Olander, R. E. Martin, and A. T. Harris, 2004: Grazing systems, ecosystem responses, and global change. *Annu. Rev. Environ. Resour.,* **29,** 261–299, doi:10.1146/annurev.energy.29.062403.102142.

Asseng, S., I. Foster, and N. C. Turner, 2011: The impact of temperature variability on wheat yields. *Global Change Biol.,* **17,** 997–1012, doi:10.1111/j.1365-2486.2010.02262.x.

——, and Coauthors, 2013: Uncertainty in simulating wheat yields under climate change. *Nat. Climate Change,* **3,** 827–832, doi:10.1038/nclimate1916.

Atkinson, M. D., P. S. Kettlewell, P. D. Hollins, D. B. Stephenson, and N. V. Hardwick, 2005: Summer climate mediates UK wheat quality response to winter North Atlantic Oscillation. *Agric. For. Meteor.,* **130,** 27–37, doi:10.1016/j.agrformet.2005.02.002.

Ball, J. T., I. E. Woodrow, and J. A. Berry, 1987: A model predicting stomatal conductance and its contribution to the control of photosynthesis under different environmental conditions. *Prog. Photosynth. Res.,* **4,** 221–224, doi:10.1007/978-94-017-0519-6_48.

Boé, J., L. Terray, F. Habets, and E. Martin, 2007: Statistical and dynamical downscaling of the Seine basin climate for hydro-meteorological studies. *Int. J. Climatol.,* **27,** 1643–1655, doi:10.1002/joc.1602.

Butler, E. E., and P. Huybers, 2013: Adaptation of US maize to temperature variations. *Nat. Climate Change,* **3,** 68–72, doi:10.1038/nclimate1585.

Cai, W., and T. Cowan, 2008: Dynamics of late autumn rainfall reduction over southeastern Australia. *Geophys. Res. Lett.,* **35,** L09708, doi:10.1029/2008GL033727.

——, and ——, 2013: Southeast Australia autumn rainfall reduction: A climate-change-induced poleward shift of ocean–atmosphere circulation. *J. Climate,* **26,** 189–205, doi:10.1175/JCLI-D-12-00035.1.

Cai, X., D. Wang, and R. Laurent, 2009: Impact of climate change on crop yield: A case study of rainfed corn in central Illinois. *J. Appl. Meteor. Climatol.,* **48,** 1868–1881, doi:10.1175/2009JAMC1880.1.

Campbell, G. S., and J. M. Norman, 1998: *An Introduction to Environmental Biophysics.* 2nd ed. Springer-Verlag, 286 pp.

Cantelaube, P., J.-M. Terres, and F. Doblas-Reyes, 2004: Influence of climate variability on Europeanagriculture—Analysis of winter wheat production. *Climate Res.,* **27,** 135–144, doi:10.3354/cr027135.

Challinor, A. J., E. S. Simelton, E. D. G. Fraser, D. Hemming, and M. Collins, 2010: Increased crop failure due to climate change: Assessing adaptation options using models and socio-economic data for wheat in China. *Environ. Res. Lett.,* **5,** doi:10.1088/1748-9326/5/3/034012.

Collatz, G. J., M. Ribas-Carbo, and J. A. Berry, 1992: Coupled photosynthesis-stomatal conductance model for leaves of C4 plants. *Aust. J. Plant Physiol.,* **19,** 519–538, doi:10.1071/PP9920519.

Compo, G. P., J. S. Whitaker, and P. D. Sardeshmukh, 2006: Feasibility of a 100-year reanalysis using only surface pressure data. *Bull. Amer. Meteor. Soc.,* **87,** 175–190, doi:10.1175/BAMS-87-2-175.

Dai, A., 2013: Increasing drought under global warming in observations and models. *Nat. Climate Change,* **3,** 52–58, doi:10.1038/nclimate1633.

——, K. E. Trenberth, and T. R. Karl, 1998: Global variations in droughts and wet spells: 1900–1995. *Geophys. Res. Lett.,* **25,** 3367–3370, doi:10.1029/98GL52511.

Donner, S. D., and C. J. Kucharik, 2008: Corn-based ethanol production compromises goal of reducing nitrogen export by the Mississippi River. *Proc. Natl. Acad. Sci. USA,* **105,** 4513–4518, doi:10.1073/pnas.0708300105.

——, M. T. Coe, J. D. Lenters, T. E. Twine, and J. A. Foley, 2002: Modeling the impact of hydrological changes on nitrate transport

in the Mississippi River Basin from 1955 to 1994. *Global Biogeochem. Cycles,* **16,** 16-1–16-19, doi:10.1029/2001GB001396.

DEPI, 2012: Growing wheat. Department of Environment and Primary Industries Tech. Note AG0548. [Available online at http://www.depi.vic.gov.au/agriculture-and-food/grains-and-other-crops/crop-production/growing-wheat.]

FAO, cited 2012: FertiStat Fertilizer Use Statistics. [Available online at http://www.fao.org/ag/agp/fertistat/index_en.htm.]

Farquhar, G. D., and T. D. Sharkey, 1982: Stomatal conductance and photosynthesis. *Annu. Rev. Plant Physiol.,* **33,** 317–345, doi:10.1146/annurev.pp.33.060182.001533.

——, S. von Caemmerer, and J. A. Berry, 1980: A biochemical model of photosynthetic CO_2 assimilation in leaves of C_3 species. *Planta,* **149,** 78–90, doi:10.1007/BF00386231.

Ferris, R., R. H. Ellis, T. R. Wheeler, and P. Hadley, 1998: Effect of high temperature stress at anthesis on grain yield and biomass of field-grown crops of wheat. *Ann. Bot.,* **82,** 631–639, doi:10.1006/anbo.1998.0740.

Foley, J. A., I. C. Prentice, N. Ramankutty, S. Levis, D. Pollard, S. Sitch, and A. Haxeltine, 1996: An integrated biosphere model of land surface processes, terrestrial carbon balance, and vegetation dynamics. *Global Biogeochem. Cycles,* **10,** 603–628, doi:10.1029/96GB02692.

——, and Coauthors, 2005: Global consequences of land use. *Science,* **309,** 570–574, doi:10.1126/science.1111772.

French, R. J., and J. E. Schultz, 1984: Water use efficiency of wheat in a Mediterranean-type environment. I. The relation between yield, water use and climate. *Aust. J. Agric. Res.,* **35,** 743–764, doi:10.1071/AR9840743.

Gudmundsson, L., J. B. Bremnes, J. E. Haugen, and T. Engen-Skaugen, 2012: Technical note: Downscaling RCM precipitation to the station scale using statistical transformations—A comparison of methods. *Hydrol. Earth Syst. Sci.,* **16,** 3383–3390, doi:10.5194/hess-16-3383-2012.

Hatfield, J., 2012: Agriculture in the Midwest. Great Lakes Integrated Sciences and Assessment Tech. Rep., 8 pp. [Available online at http://glisa.umich.edu/media/files/NCA/MTIT_Agriculture.pdf.]

Hulme, M., 1992: A 1951–80 global land precipitation climatology for the evaluation of general circulation models. *Climate Dyn.,* **7,** 57–72, doi:10.1007/BF00209609.

——, 1994: Validation of large-scale precipitation fields in general circulation models. *Global Precipitations and Climate Change,* M. Desbois and F. Désalmand, Eds., NATO ASI Series, Vol. 26, Springer-Verlag, 387–406, doi:10.1007/978-3-642-79268-7_25.

IGBP, cited xxxx: Global soil data products CD-ROM (IGBP-DIS). International Geosphere-Biosphere Programme Tech. Rep. [Available online at http://daac.ornl.gov/SOILS/guides/igbp.html.]

Iizumi, T., and Coauthors, 2014: Historical changes in global yields: Major cereal and legume crops from 1982 to 2006. *Glob. Ecol. Biogeogr.,* **23,** 346–357, doi:10.1111/geb.12120.

IPCC, 2013: Summary for policymakers. *Climate Change 2013: The Physical Science Basis,* T. F. Stocker et al., Eds., Cambridge University Press, 3–29. [Available online at http://www.ipcc.ch/pdf/assessment-report/ar5/wg1/WG1AR5_SPM_FINAL.pdf.]

Kalnay, E., and Coauthors, 1996: The NCEP/NCAR 40-Year Reanalysis Project. *Bull. Amer. Meteor. Soc.,* **77,** 437–471, doi:10.1175/1520-0477(1996)077<0437:TNYRP>2.0.CO;2.

Kistler, R., and Coauthors, 2001: The NCEP–NCAR 50-Year Reanalysis: Monthly means CD-ROM and documentation. *Bull. Amer. Meteor. Soc.,* **82,** 247–267, doi:10.1175/1520-0477(2001)082<0247:TNNYRM>2.3.CO;2.

Kucharik, C. J., 2003: Evaluation of a process-based agro-ecosystem model (Agro-IBIS) across the U.S. Corn Belt: Simulations of the interannual variability in maize yield. *Earth Interact.,* **7,** 1–33, doi:10.1175/1087-3562(2003)007<0001:EOAPAM>2.0.CO;2.

——, and K. R. Brye, 2003: Integrated Biosphere Simulator (IBIS) yield and nitrate loss predictions for Wisconsin maize receiving varied amounts of nitrogen fertilizer. *J. Environ. Qual.,* **32,** 247–268, doi:10.2134/jeq2003.2470.

——, and N. Ramankutty, 2005: Trends and variability in U.S. corn yields over the twentieth century. *Earth Interact.,* **9,** 1–29, doi:10.1175/EI098.1.

——, and T. E. Twine, 2007: Residue, respiration, and residuals: Evaluation of a dynamic agroecosystem model using eddy flux measurements and biometric data. *Agric. For. Meteor.,* **146,** 134–158, doi:10.1016/j.agrformet.2007.05.011.

——, and Coauthors, 2000: Testing the performance of a dynamic global ecosystem model: Water balance, carbon balance, and vegetation structure. *Global Biogeochem. Cycles,* **14,** 795–825, doi:10.1029/1999GB001138.

Leakey, A. D. B., M. Uribelarrea, E. A. Ainsworth, S. L. Naidu, A. Rogers, D. R. Ort, and S. P. Long, 2006: Photosynthesis, productivity, and yield of maize are not affected by open-air elevation of CO_2 concentration in the absence of drought. *Plant Physiol.,* **140,** 779–790, doi:10.1104/pp.105.073957.

Lobell, D. B., and G. P. Asner, 2003: Climate and management contributions to recent trends in US agricultural yields. *Science,* **299,** 1032, doi:10.1126/science.1077838.

——, and C. B. Field, 2007: Global scale climate–crop yield relationships and the impacts of recent warming. *Environ. Res. Lett.,* **2,** 014002, doi:10.1088/1748-9326/2/1/014002.

——, and ——, 2008: Estimation of the CO_2 fertilization effect using growth rate anomalies of CO_2 and crop yields since 1961. *Global Change Biol.,* **14,** 451, doi:10.1111/j.1365-2486.2007.01536.x.

——, M. Bänziger, C. Magorokosho, and B. Vivek, 2011a: Nonlinear heat effects on African maize as evidenced by historical yield trials. *Nat. Climate Change,* **1,** 42–45, doi:10.1038/nclimate1043.

——, W. Schlenker, and J. Costa-Roberts, 2011b: Climate trends and global crop production since 1980. *Science,* **333,** 616–620, doi:10.1126/science.1204531.

——, A. Sibley, and J. I. Ortiz-Monasterio, 2012: Extreme heat effects on wheat senescence in India. *Nat. Climate Change,* **2,** 186–189, doi:10.1038/nclimate1356.

——, G. L. Hammer, G. McLean, C. Messina, M. J. Roberts, and W. Schlenker, 2013: The critical role of extreme heat for maize production in the United States. *Nat. Climate Change,* **3,** 497–501, doi:10.1038/nclimate1832.

Malone, R. W., D. W. Meek, J. L. Hatfield, M. E. Mann, R. J. Jaquis, and L. Ma, 2009: Quasi-biennial corn yield cycles in Iowa. *Agric. For. Meteor.,* **149,** 1087–1094, doi:10.1016/j.agrformet.2009.01.009.

McGrath, J. M., and D. B. Lobell, 2011: An independent method of deriving the carbon dioxide fertilization effect in dry conditions using historical yield data from wet and dry years. *Global Change Biol.,* **17,** 2689–2696, doi:10.1111/j.1365-2486.2011.02406.x.

Mehta, V. M., N. J. Rosenberg, and K. Mendoza, 2012: Simulated impacts of three decadal climate variability phenomena on dryland corn and wheat yields in the Missouri River Basin. *Agric. For. Meteor.,* **152,** 109–124, doi:10.1016/j.agrformet.2011.09.011.

Miller, D. A., and R. A. White, 1998: A conterminous United States multilayer soil characteristics dataset for regional

climate and hydrology modeling. *Earth Interact.,* **2,** 1–26, doi:10.1175/1087-3562(1998)002<0001:ACUSMS>2.3.CO;2.

Mitchell, T. D., and P. D. Jones, 2005: An improved method of constructing a database of monthly climate observations and associated high-resolution grids. *Int. J. Climatol.,* **25,** 693–712, doi:10.1002/joc.1181.

Moss, R. H., and Coauthors, 2010: The next generation of scenarios for climate change research and assessment. *Nature,* **463,** 747–756, doi:10.1038/nature08823.

Neild, R. E., and J. E. Newman, 1987: Growing season characteristics and requirements in the Corn Belt. Iowa State University Cooperative Extension Service and National Corn Handbook Rep. NCH-40.

New, M., M. Hulme, and P. Jones, 1999: Representing twentieth-century space–time climate variability. Part I: Development of a 1961–90 mean monthly terrestrial climatology. *J. Climate,* **12,** 829–856, doi:10.1175/1520-0442(1999)012<0829:RTCSTC>2.0.CO;2.

Nicholls, N., 1985: Impact of the southern oscillation on Australian crops. *J. Climatol.,* **5,** 553–560, doi:10.1002/joc.3370050508.

——, 1997: Increased Australian wheat yield due to recent climate trends. *Nature,* **387,** 484–485, doi:10.1038/387484a0.

Patricola, C. M., and K. H. Cook, 2013: Mid-twenty-first century warm season climate change in the Central United States. Part I: Regional and global model predictions. *Climate Dyn.,* **40,** 551–568, doi:10.1007/s00382-012-1605-8.

Perkins, S. E., A. J. Pitman, and S. A. Sisson, 2009: Smaller projected increases in 20-year temperature returns over Australia in skill-selected climate models. *Geophys. Res. Lett.,* **36,** L06710, doi:10.1029/2009GL037293.

Persson, T., A. Garcia y Garcia, J. Paz, J. Jones, and G. Hoogenboom, 2009: Maize ethanol feedstock production and net energy value as affected by climate variability and crop management practices. *Agric. Syst.,* **100,** 11–21, doi:10.1016/j.agsy.2008.11.004.

Pitman, A. J., and S. E. Perkins, 2008: Regional projections of future seasonal and annual changes in rainfall and temperature over Australia based on skill-selected AR4 models. *Earth Interact.,* **12,** 1–50, doi:10.1175/2008EI260.1.

Pook, M., S. Lisson, J. Risbey, C. C. Ummenhofer, P. McIntosh, and M. Rebbeck, 2009: The autumn break for cropping in southeast Australia: Trends, synoptic influences and impacts on yield. *Int. J. Climatol.,* **29,** 2012–2026, doi:10.1002/joc.1833.

Porter, J. R., and M. Gawith, 1999: Temperatures and the growth and development of wheat: A review. *Eur. J. Agron.,* **10,** 23–36, doi:10.1016/S1161-0301(98)00047-1.

——, and M. A. Semenov, 2005: Crop responses to climatic variation. *Philos. Trans. Roy. Soc. London,* **360B,** 2021–2035, doi:10.1098/rstb.2005.1752.

Potgieter, A., H. Meinke, A. Doherty, V. O. Sadras, G. Hammer, S. Crimp, and D. Rodriguez, 2013: Spatial impact of projected changes in rainfall and temperature on wheat yields in Australia. *Climatic Change,* **117,** 163–179, doi:10.1007/s10584-012-0543-0.

Power, S., T. Casey, C. Folland, A. Colman, and V. Mehta, 1999: Inter-decadal modulation of the impact of ENSO on Australia. *Climate Dyn.,* **15,** 319–324, doi:10.1007/s003820050284.

Ramankutty, N., and J. A. Foley, 1999: Estimating historical changes in land cover: North American croplands from 1850 to 1992. *Global Ecol. Biogeogr.,* **8,** 381–396, doi:10.1046/j.1365-2699.1999.00141.x.

Riahi, K., and Coauthors, 2011: RCP 8.5—A scenario of comparatively high greenhouse gas emissions. *Climatic Change,* **109,** 33–57, doi:10.1007/s10584-011-0149-y.

Sacks, W. J., and C. J. Kucharik, 2011: Crop management and phenology trends in the U.S. Corn Belt: Impacts on yields, evapotranspiration and energy balance. *Agric. For. Meteor.,* **151,** 882–894, doi:10.1016/j.agrformet.2011.02.010.

Sánchez, B., A. Rasmussen, and J. R. Porter, 2014: Temperatures and the growth and development of maize and rice: A review. *Global Change Biol.,* **20,** 408–417, doi:10.1111/gcb.12389.

Schaefer, K., and Coauthors, 2012: A model-data comparison of gross primary productivity: Results from the North American Carbon Program site synthesis. *J. Geophys. Res.,* **117,** G03010, doi:10.1029/2012JG001960.

Schlenker, W., and M. J. Roberts, 2009: Nonlinear temperature effects indicate severe damage to U.S. crop yields under climate change. *Proc. Natl. Acad. Sci. USA,* **106,** 15 594–15 598, doi:10.1073/pnas.0906865106.

Southworth, J., J. C. Randolph, M. Habeck, O. C. Doering, R. A. Pfeifer, D. G. Rao, and J. J. Johnston, 2000: Consequences of future climate change and changing climate variability on maize yields in the midwestern United States. *Agric. Ecosyst. Environ.,* **82,** 139–158, doi:10.1016/S0167-8809(00)00223-1.

——, R. A. Pfeifer, M. Habeck, J. C. Randolph, O. C. Doering, J. J. Johnston, and D. G. Rao, 2002: Changes in soybean yields in the midwestern United States as a result of future changes in climate, climate variability, and CO_2 fertilization. *Climatic Change,* **53,** 447–475, doi:10.1023/A:1015266425630.

Stephens, D. J., and T. J. Lyons, 1998: Variability and trends in sowing dates across the Australian wheatbelt. *Aust. J. Agric. Res.,* **49,** 1111–1118, doi:10.1071/A96173.

Timbal, B., and W. Drosdowsky, 2013: The relationship between the decline of southeastern Australian rainfall and the strengthening of the subtropical ridge. *Int. J. Climatol.,* **33,** 1021–1034, doi:10.1002/joc.3492.

Twine, T. E., and C. J. Kucharik, 2008: Evaluating a terrestrial ecosystem model with satellite information of greenness. *J. Geophys. Res.,* **113,** G03027, doi:10.1029/2007JG000599.

——, and ——, 2009: Climate impacts on net primary productivity trends in natural and managed ecosystems of the central and eastern United States. *Agric. For. Meteor.,* **149,** 2143–2161, doi:10.1016/j.agrformet.2009.05.012.

——, J. J. Bryant, K. T. Richter, C. J. Bernacchi, K. D. McConnaughay, S. J. Morris, and A. D. B. Leakey, 2013: Impacts of elevated CO_2 concentration on the productivity and surface energy budget of the soybean and maize agroecosystem in the Midwest USA. *Global Change Biol.,* **19,** 2838–2852, doi:10.1111/gcb.12270.

USDA, cited 2013: Table 10: Nitrogen used on corn, rate per fertilized acre receiving nitrogen, selected States, 1964–2010. [Available online at http://www.ers.usda.gov/data-products/fertilizer-use-and-price.]

USDA-NASS, 2009: 2007 Census of agriculture, volume 1. National Agricultural Statistics Service Tech. Rep. AC-07-A-51, 639 pp. [Available online at http://www.agcensus.usda.gov/Publications/2007/Full_Report/usv1.pdf.]

VanLoocke, A., C. J. Bernacchi, and T. E. Twine, 2010: The impacts of *Miscanthus×giganteus* production on the Midwest US hydrologic cycle. *Global Change Biol. Bioenergy,* **2,** 180–191, doi:10.1111/j.1757-1707.2010.01053.x.

——, T. E. Twine, M. Zeri, and C. J. Bernacchi, 2012: A regional comparison of water use efficiency for miscanthus, switchgrass and maize. *Agric. For. Meteor.,* **164,** 82–95, doi:10.1016/j.agrformet.2012.05.016.

Wang, E., J. Xu, Q. Jiang, and J. Austin, 2009: Assessing the spatial impact of climate on wheat productivity and the potential value of climate forecasts at a regional level. *Theor. Appl. Climatol.,* **95,** 311–330, doi:10.1007/s00704-008-0009-5.

Wang, J., E. Wang, and D. L. Liu, 2011: Modelling the impacts of climate change on wheat yield and field water balance over the Murray–Darling Basin in Australia. *Theor. Appl. Climatol.,* **104,** 285–300, doi:10.1007/s00704-010-0343-2.

Wardlaw, I. F., and C. W. Wright, 1994: Heat tolerance in temperate cereals: An overview. *Aust. J. Plant Physiol.,* **21,** 695–703, doi:10.1071/PP9940695.

Webler, G., D. R. Roberti, S. V. Cuadra, V. S. Moreira, and M. H. Costa, 2012: Evaluation of a dynamic agroecosystem model (Agro-IBIS) for soybean in southern Brazil. *Earth Interact.,* **16,** 1–15, doi:10.1175/2012EI000452.1.

Wheeler, T., and J. von Braun, 2013: Climate change impacts on global food security. *Science,* **341,** 508–513, doi:10.1126/science.1239402.